THERMAL DEBINDING OF

METAL INJECTION MOLDED PARTS WITH AN AGAR-GEL

BINDER SYSTEM

THERMAL DEBINDING OF

METAL INJECTION MOLDED PARTS WITH AN AGAR-GEL

BINDER SYSTEM

By

XIAOYUN LI

A Thesis

Submitted to the School of Graduate Studies

In Partial Fulfillment of the Requirements

For the Degree

Master of Applied Science

McMaster University

MASTER OF APPLIED SCIENCE (2007)   McMaster University

(Chemical Engineering)   Hamilton, Ontario

TITLE: Thermal Debinding of Metal Injection Molded Parts with an

                          Agar-gel Binder System

AUTHOR: Xiaoyun Li

                          B. Eng. (Sichuan University)

SUPERVISOR: Dr. Andrew Hrymak

                          McMaster University

NUMBER OF PAGES: xi, 91

ABSTRACT

Metal injection molding (MIM) employs the advantages of injection molding and powder metallurgy and provides a high productivity means to form intricate, low-cost, high performance metal parts. One of the most unique characteristics of MIM is the binder system and the consequent debinding step, which is considered to be major process improvement barrier in the MIM process. A MIM part with a thick section suffers from a long debinding cycle and it is difficult to avoid defects. Therefore, it is always of interest to find out a method to quickly debind a thick part without defects.

PowderFlo® feedstock combines metal powder with an aqueous agar-gel binder system and requires simple air-drying followed by thermal debinding. However, previous studies on this agar-gel binder feedstock mainly focus on sintering, while the debinding step has lacked sufficient attention.

A debinding study on agar-gel binder system is conducted in the present project. The metal compacts are formed via compression molding and injection molding, followed with thermal debinding in order to understand the effects of process parameters on debinding with respect to thickness to determine a good debinding schedule. The thickness transition between thick and thin section is particularly important in the debinding to find a protocol to make parts with both thick and thin sections.

Thermal debinding experiments show that the initial heating rate is the most significant factor due to it may cause visible defect directly and an increase of initial and secondary heating rates may retard binder removal. The air-drying time has less influence

on binder extraction for thicker section. Extending the holding time for water and polymer removal is beneficial to obtain better dimensional control. The overall debinding process parameters have larger effects on thicker parts. For the thickness transition, it is suggested to avoid the combination of too thin and too thick section, increase the joint area, and provide uniform packing during molding.

ACKNOWLEDGEMENTS

TABLE OF CONTENTS

LIST OF FIGURES

LIST OF TABLES

Chapter 1

INTRODUCTION

1.1 Metal Injection Molding

Injection molding is one of the most commonly used technologies in plastics manufacturing industries. In the 1980's, injection molding was widely commercially applied to metal powders in addition to polymers and developed rapidly as a new technology known as metal injection molding (MIM). Accordingly metal injection molding employs the advantages of both injection molding and powder metallurgy.

The process of MIM starts with the mixing of metal powders and polymeric binders to form a feedstock, which then is fed into an injection molding machine. The injection molded part is termed as a "green" part. The binders are extracted by either a solvent extraction or thermal debinding step (named as a "brown" part) and the remaining powder is sintered for densification. Finally, the desired net-shape metal part is obtained after sintering. The MIM process consists of four process steps: feedstock mixing, injection molding, debinding and sintering. Each of steps plays a specific and important role in successful metal injection molding.

The most unique characteristic in MIM is the binder system and the consequent debinding step, compared with other conventional metal manufacturing techniques. The binder provides the flowability and moldability to feedstock and makes it easy for shape forming, while the binder must be removed with least residue remaining in the component and maintaining the required part shape prior to sintering. Thus the debinding

1

step is generally considered to be the major barrier in improving productivity of the MIM process. Furthermore, the key factor to economic success of MIM is the thickness of the component because a MIM part with large volume or thick section requires very long time to debind and it is difficult to avoid defects during debinding. For instance, cracking, blisters, and shape distortion are common defects occurring during the debinding step. Therefore it is always of interest for industries to debind a thick or large part free of defects in a time-efficient manner.

1.2 Agar-gel Binder System

In the past decade, an aqueous agar-based binder feedstock (Ballard and Zedalis, 1998) has been developed which requires simple air-drying at ambient temperature followed by high temperature thermal debinding. This makes it possible to debind larger (>200 gram) or thicker (>6 mm) parts by using short time oven drying where it is very difficult to debind in a time efficient manner with other MIM feedstock systems (Wick et al., 2003). Moreover, it has been reported that net-shape stainless steel components as large as 2 kilogram have been obtained by using an agar-gel binder system (LaSalle and Zedalis, 1999). The viscosity of feedstock has a magnitude of 10^3 Pa·S and is similar to that of unfilled Nylon-6 during injection molding. The green part is placed in the ambient air as the initial debinding stage for water removal. In later debinding stages, the polymer removal is incorporated into the pre-sintering step.

The feedstock consists of agar (which is a type of polysaccharide derived from seaweed), metal powder, water and a gel strength-enhancing agent which has the form of

borate compound such as calcium borate, zinc borate, etc. (Fanelli, 1998). The use of agar-gel with the gel strength enhancing additive can reduce the binder content (typically 2-3 wt %) needed for shape retention (MPR, 2006). Hence, the as-molded parts have higher green strength and deformation resistance with a lower binder percentage. Water not only plays a role similar to solvent but also the carrier for agar containing mixtures. In addition, the feedstock may also employ various additives in order to meet other requirements, for example, dispersant and biocides. The metal powder is usually produced by gas-atomization and the typical particle size is less than 20 micrometers. Due to the lower binder content this feedstock has higher solids loading, which leads to less shrinkage after densification and as a result, improved dimensional control. The solids loading of feedstock is nearly 92 wt% (61 vol %), water content is around 7.5 wt%, and the balance is other binder materials.

Compared with traditional plastics injection molding, water-based agar gel binder feedstock can be molded at a lower process temperature and pressure, but it has much longer cycle time depending on the part size/thickness. These molded parts have approximately 2% shrinkage during air-drying and 17% shrinkage during the sintering process.

Due to its unique character, the aqueous agar gel binder system has attracted considerable interest. Most researchers have focused on the sintering step, which involves sintering densification, simulation of sintering densification and shrinkage behaviour (Kwon, et al. 2004; Wu, et al. 2002a; Wu, et al. 2002b).

3

1.3 Objective

The objective of the present work is to understand the role of debinding process parameters in order to determine the appropriate debinding path with respect to size/thickness of a MIM part. The metal components are formed by compression and injection molding, and then the intermediate parts are debound via various thermal treatments. According to part weight and dimensional changes, the parts are assessed after debinding and then some of the debound parts are selected for sintering. The thickness transition between thin and thick sections is a major concern because major defects may occur in the transition area. Therefore, the thickness transition is also investigated. Generally, an improper thermal debinding time-temperature schedule is the main source of defects.

1.4 Outline

Chapter 2 is devoted to the review of metal injection molding with emphasis on the binder system and debinding techniques. Some simulation models of the debinding process are briefly summarized. Chapter 3 describes the materials used, process equipment, and the experimental steps (compression molding, injection molding, thermal debinding and sintering). Chapter 4 analyzes the effect of different process variables on the debinding and discusses the debinding schedule with respect to time and part thickness. Chapter 5 summarizes the conclusions and recommends some future works.

Chapter 2

LITERATURE REVIEW

Compared with the amount of research on feedstock composition, injection molding, and sintering of MIM process, debinding has not had similar attention although it is a critical step in MIM. This chapter will summarize the research focusing on debinding in recent decades. An overview is presented about MIM technology, then the research on metal powder, binder, and debinding simulation models are discussed.

2.1 Overview of Metal Injection Molding

Metal injection molding is a competitive manufacturing technique for the fabrication of high performance metal products with complicated geometry. The main advantages of MIM are:

1. Metals have superior properties over polymers, such as higher strength, stiffness etc. MIM part overcomes the property restrictions inherent to polymers.

2. Polymeric binders provide good flowability and moldability that make it possible to form complex shapes.

3. Tight tolerance, i.e. ± 0.5% of nominal, is able to achieve without post machining if the mold is well designed.

4. MIM offers low cost especially for large quantity production. The more products that are produced, the lower price for each can be obtained if fixed costs can be distributed over more products.

5. MIM is applicable to many metal materials so that various properties can be achieved.

6. Feedstock materials can be recycled in accordance to cost and environmental requirements.

The MIM process involves four process procedures: feedstock mixing, injection molding, debinding, and sintering, as shown in Figure 2.1. In the following sections, each of the process steps will be introduced.

2.1.1 Feedstock Mixing

In the first stage, the metal powder is mixed with polymeric binder until a homogenous compound is obtained, and then the feedstock is granulated.

Important characteristics of the metal powders include particle size distribution, packing density, particle shape, particle fabrication method, and particle surface. (German and Bose, 1997) The ideal MIM powders should possess particles in the size range between 0.5-20μm with D_{50} between 4-8μm, desired particle size distribution slope parameter S_w[1] = 2 or 8, tap density[2] over 50% of theoretical, nearly spherical shape, dense particles without voids, clean surface and minimum segregation.

Generally the binder system contains thermoplastics or thermosetting polymers, wetting agents, mold release agents and other additives to fulfill three tasks:

- Sufficient flowability and moldability for injection molding

---

[1] . $S_w = 2.56/((\log_{10} (D_{90}/D_{10}))$

[2] Tap density is the highest density that can be achieved by vibrating a powder

6

- Necessary strength for handling prior to pre-sintering

- Easily extracted from the parts with minimum residue.
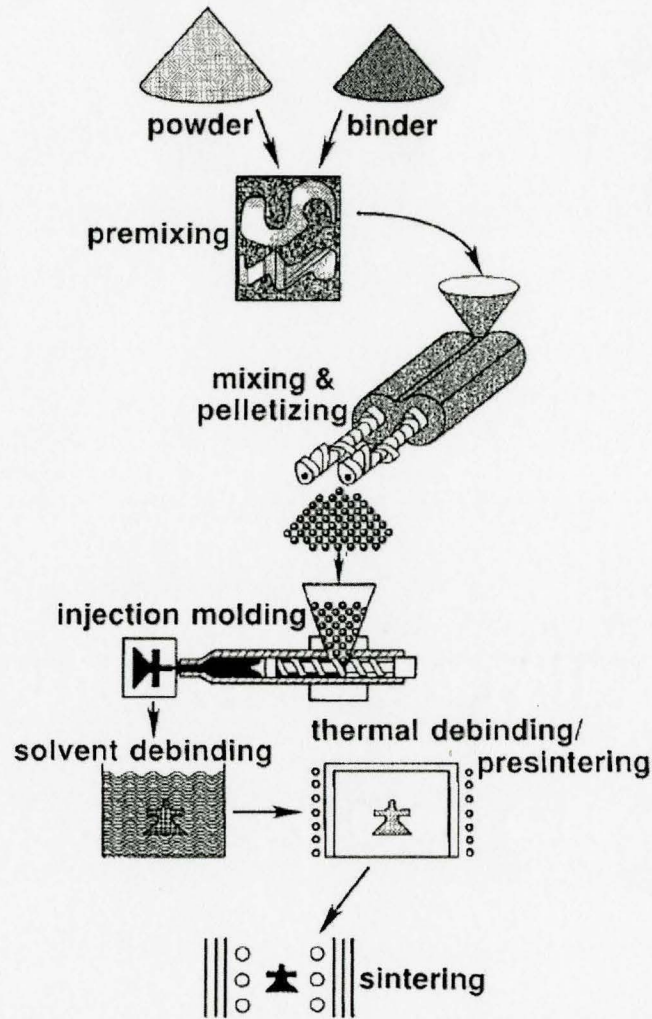
Figure 2.1 Schematic diagram of MIM process (German, 1997)

The solids loading, volumetric ratio of solid powder to total volume of powder and binder is a crucial parameter for MIM feedstock due to its large effect on viscosity. A large powder to binder ratio, results in a high viscosity, insufficient flowability and difficulty in shaping the mold. If the powder to binder ratio is too low, there may be too

much binder, which makes shape retention difficult. Thus the solids loading should be decided carefully. There are a few methods available to determine the critical solids loading, such as the measurement of density, melt flow, mixing torque, and viscosity as a function of particle composition. The optimal solids loading should be slightly below the critical point because the slight excess of binder offers needed lubricity for molding.

After the feedstock recipe is determined, the feedstock ingredients are mixed together. In order to obtain the uniform mixture, the powder should disperse in the binder without interval porosity or agglomerates. Moreover, the homogeneity of feedstock should be evaluated to ensure its quality via measuring the viscosity and its variation during testing.

2.1.2 Injection Molding

In the second stage, the feedstock is injection molded similar to conventional thermoplastic injection molding. The feedstock is heated until it melts to fill the cavity, then pressure is applied on the resin until the part is cooled down. After cooling, the part is ejected as a "green part".

During the molding stage, process parameters such as barrel, nozzle, and mold temperatures; pressure gradient; and filling, packing, and cooling stage times play important roles for good-quality products. The appropriate process control should not only be able to provide sufficient flow of the feedstock to fill the cavity and shorten the molding cycle but also produce parts free of defects.

2.1.3 Debinding

In the third stage, the binder is extracted from the green part. The debound part is called a "brown part". The objective of debinding is to remove most of the binder with minimal remaining residue in the shortest time. Removal of binder is generally divided into multiple steps based on the formulation. The removal of initial binder component provides a porous structure that facilitates the rest of the binder components to diffuse to the part surface. When the extractable binder components are completely removed, the part becomes friable so that it is not easy to maintain the shape and handle to sintering stage. Therefore the final step of debinding is also regarded as presintering.

Various debinding techniques have been developed using thermal, solvent and catalytic debinding processes. The most common process methods are shown in Figure 2.2 (Hwang, 1996). These methods as well as other approaches such as supercritical CO_2 extraction, crosslinked polymer binder, water debinding etc. will be discussed below.

Thermal debinding in ambient air is the oldest approach and still used widely due to the simple requirement for the equipment. Vacuum-thermal debinding is used because low pressure or vacuum can increase the debinding rate, especially for low molecular weight binder components that normally have a high vapor pressure. A problem in air thermal debinding is that it generates oxides on the metal powder surfaces, which might prohibit subsequent sintering, and the carbon content which affects the performance of the final product significantly. Accordingly, a reducing or inert atmosphere is applied to replace the oxidizing atmosphere in some cases. Fine powder (wicking) can also speed up the binder removal due to its high negative capillary pressure. But it is difficult to clean

the compact surface containing the wicking powder. Solvent debinding is based on the binder system that contains a filler component (such as wax), which is soluble in solvent, a backbone component (such as thermoplastic), which is insoluble and lubricant component. Solvent-thermal debinding is superior to other debinding methods because of shorter debinding cycle and better shape retention. The solvent debinding method includes immersing the parts in a liquid solvent and exposing the part in solvent vapor. But the liquid solvent concentration changes with the immersion time, which can affect the debinding rate, while vapor solvent debinding has slow dissolution ability. These drawbacks can be overcome by using condensed vapor in order to increase the dissolution rate and debinding rate. Another inherent disadvantage of solvent debinding is the environmental issues such as solvent storage and handling. Water has been used to replace organic solvents in water-soluble binder system that has been developed. Water is used to leach the soluble binder component and then dried prior to thermal debinding. In the catalytic debinding process, the reactive component such as modified polyacetal is used as base binder and depolymerized into formaldehyde, and then the remaining component is pyrolyzed. There is no liquid phase, but only a solid-gas reaction in this process. As a result, catalytic debinding has very good shape retention capability and a fast debinding rate. Its main disadvantage involves comparatively lower solids loading, which might lead to larger shrinkage. Supercritical fluids (typically carbon dioxide) have specific physical properties between gas phase and liquid state. An example of supercritical debinding (Shimizu, et al. 2001) is to extract binder (75% Paraffin Wax + 20% Polyethylene + 5% Ethylene Vinyl Acetate copolymer in weight) from a green part

in CO_2 using a pressure as 20 MPa and a temperature as 45 °C. Thus the soluble binder component (PW) is dissolved in supercritical CO_2 while the rest of the binder components (PE + EVA) hold the part shape. This approach has a faster debinding rate than solvent or thermal debinding and less defect sources. Thermosetting polymers are good at keeping the part shape during molding and debinding so that it has been developed to be binder component. Thus the initial debinding can be achieved prior to ejecting parts from the heated mold. The rest of the binder can be removed rapidly by thermal treatment. This debinding method for thermoset binder systems exhibits fast debinding cycles but a long overall molding cycle.

Whatever debinding method is chosen, the debinding rate is the key to good quality of the brown part. In practice, the main problem is the lengthy debinding time and defects that occurs due to debinding.

2.1.4 Sintering

Sintering is the thermal treatment by heating the brown part to the temperature just below its melting point until the metal particles adhere to each other. Thus the pores are eliminated as part of particle bonding during sintering and the brown part shrinks to smaller size with the normal shrinkage of 10-20 % (German and Bose, 1997). During the pore elimination, the mass flows along particle surface, pore space, grain boundaries, and the interconnected interior. Therefore the sintering mechanisms consist of surface diffusion, evaporation-condensation, volume diffusion and grain boundary diffusion.
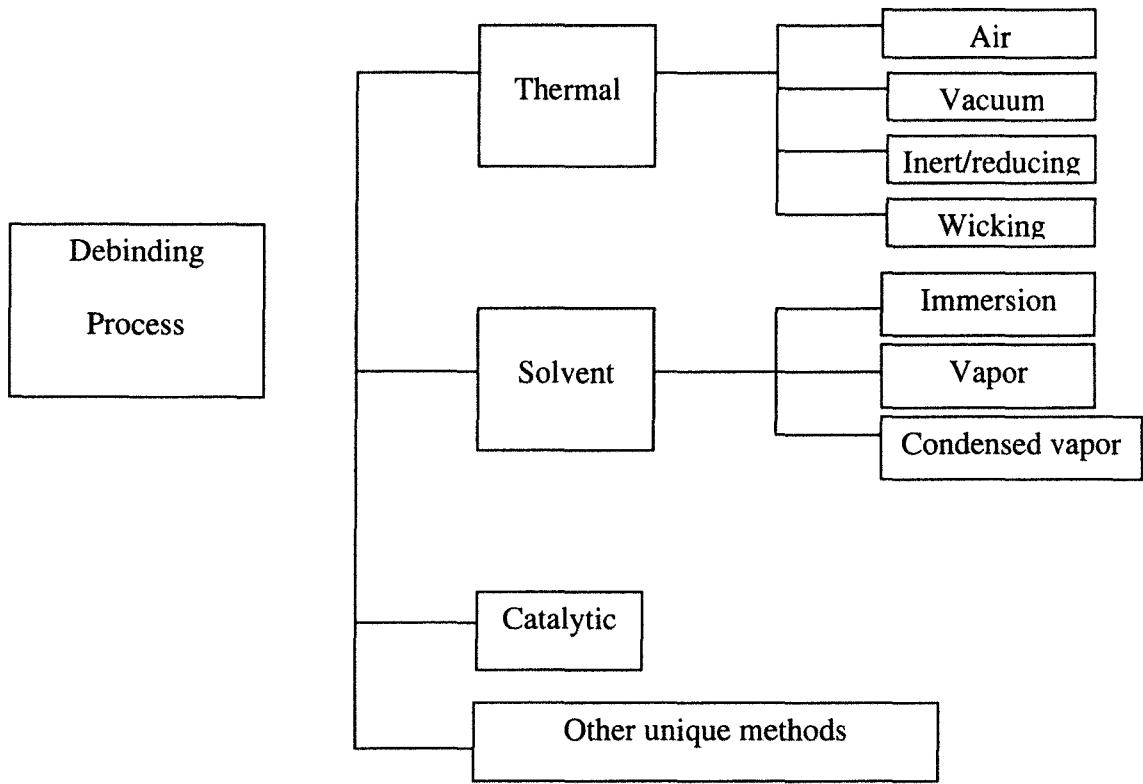
Figure 2.2 Types of debinding process (Hwang, 1996)

A good sintering cycle for densification through microstructure control might consist of rapid heating at relatively low temperatures, and slow heating in the intermediate temperature and a final short holding time at high temperature. The main driving force for sintering is the surface tension associated with the curved surface, which is determined by the process parameters and material properties, such as heating rate, temperature, particle size, grain size, and external pressure.

One important indicator of sintering is compact density. The final density of a sintered part generally reaches 95-100% of theoretical density. Another indicator of

sintering is linear dimensional change, namely the ratio of the difference in dimension to the original dimension.

Sintering is the final stage in MIM however, it is unable to correct the defects resulting from previous steps like feedstock mixing, molding, or debinding. On the contrary, many defects that are invisible in the previous stages become noticeable. Therefore each of the process stages should be in good control in order to obtain MIM products free of defects.

2.2 Metal Powder

The metal powder is the fundamental ingredient in MIM feedstock and mainly fabricated by water-atomization and gas-atomization techniques. Compared to water-atomized metal powders, the gas-atomized metal powders have the advantage of low shrinkage and distortion due to the spherical shape with smaller particle size, but the lower cost and higher debound strength of water-atomized powders have drawn some researchers' attention. Koseski et al. (2005) investigated the microstructural evolution and densification behavior of water- and gas-atomized 316L stainless steel powder, which have similar particle size and particle size distribution by conducting dilatometry and quenching experiments. Water-atomized powder with 53% solids loading can be sintered to 97% of theoretical density at 1350 °C exhibiting 21% shrinkage, while the gas-atomized powder with 65% solids loading has more than 99% of theoretical density showing 15% shrinkage. Koseski et al. (2005) explained that the difference in densification behavior was due to the oxygen content rather than the powder morphology.

The oxygen analysis of the sintered products showed 0.196 wt% of oxygen in the water-atomized powder and only 0.0009 wt % for the gas-atomized powder. Above 1250°C, the H_2O is generated and should be diffuse out, but H_2O is trapped within the pore when the compact is in closed porosity condition. Therefore, the trapped H_2O within the closed pores results in the different densification behavior of these two types of powders.

In addition 17-4 PH is another widely used stainless steel. German (1997) compared the characteristics of 17-4PH stainless steel of water-atomized, gas-atomized and slightly particle shape modified (by milling) water-atomized powders mixing with two binders in injection molding. The mixing torque tests showed that milling facilitates in increasing the solids loading while maintaining a low mixture viscosity. Although the viscosity is higher than the spherical gas-atomized powder, the milled water-atomized powders exhibited satisfactory behavior during injection molding. In the sintering stage, above a temperature of 1250°C, the milled water-atomized powder had the highest sintered density.

Although over 50% of the injection molded metal components are made from steel compositions, other metals and their powder production methods are of interest. Hartwig et al. (1998) studied the specifications and resulting properties of tungsten heavy alloy, titanium, intermetallics including NiAlCr and $MoSi_2$, as well as stainless steel. As a refractory metal, niobium was developed to form the feedstock for MIM. Aggarwal et al. (2006) first applied the niobium feedstock into the MIM process and determined the optimal solids loading based on rheological behavior. Loh et al. (2001) proposed the metal matrix composites (MMCs), which consist of 316L stainless steel and TiC

14

powders, and found that the addition of TiC can improve the microhardness and density of the final product free of defects. Huang et al. (2003a) applied the nano-technology into metal injection molding. The nano-crystalline powder of W-Ni-Fe alloy was prepared by mechanical alloying and mixed with wax-based binder. The experiments indicated that the milling of W-Ni-Fe powder results in higher density and strength while the composite has better flowability, moldability and sinterability. Huang et al. (2003b) also studied the rheology of the feedstock mixing Fe/Ni powders with several binders and an equation was established to describe the relation of temperature, shear rate and viscosity under constant powder loading.

2.3 Binders

The most commonly used debinding approaches are summarized and listed in Table 2.1, as well as their key features, advantages and disadvantages. These debinding methods have been developed and are applied well in practice. In the following, the research focusing on binder development in the recent decades is discussed taking into account with overcoming common defects.

Table 2.1 Debinding Approaches (German and Bose, 1997)

Debinding Techniques	Key features	Advantages	Disadvantages
Solvent Immersion	Immerse compact in solvent to extract filler component via dissolution	Well shape retention, opens pore channels for subsequent binder degradation, fast rate	Solvent hazard, chemical handling and environmental concern, drying needed
Supercritical Extraction	Dissolve binder into supercritical fluid	No phase change and minimize defect formation	High equipment requirement for temperature and pressure control, slow debinding rate
Wicking	Heat compact in fine powder or porous substrate to absorb molten binder	Fast initial rate, applicable to wide range of binder, easy to control	Distortion possible due to multiple handling steps, binder disposal problems, cleaning of part surface needed
Catalytic Depolymeriza-tion	Heat compact in atmosphere containing catalyst to decompose polymer	Rapid process, excellent shape retention for both thin and thick sections	Hot mold, possible hazards with special acid catalysts and decomposition products
Thermal Degradation	Heat compact with continual purging gas to give progressive degradation of binder	One step process, no handling needed between debinding and sintering, widely used process, low cost installation	Poor dimensional control, slow debinding rate
Oxidation	Heat compact in air to burn out binder and oxidize powder to get strength	High strength after debinding, effective in removing carbon	Low residual carbon, slow rate, poor dimensional control

Crosslinked binder systems have proven to be an effective approach for shape retention during debinding (Hens, et al., 1994). Haney (2000) applied urethane technology to develop a crosslinkable binder system for MIM that can avoid distortion such as slumping. Haney et al. (2001) also proposed a crosslinked polyethylene based binder system to stabilize the MIM feedstock and found that it has better dimensional control properties compared to a commercially available 17-4PH feedstock.

Due to increasing concerns about environmental issues, water-soluble binders have been developed to overcome the problems associated with organic solvents such as storage and handling. Moreover water-soluble binder system should be environmentally safe and have a short debinding time. Robles (2002) used water-soluble binder recipe (60% polyethylene + 35% polyethylene glycol + 5% glycerol in weight), which worked well with stainless steel 316L and showed little distortion and swelling. One of the new developments in water-soluble binders is aqueous agar gel feedstock that only requires a short air-drying debinding time at room temperature. This makes it possible to debind larger (>200g) or thicker walled parts (>6mm). Table 2.2 (Wick, 2003) compared the binder-related factors between conventional MIM binders and agar-gel binder: PowderFlo®.

The PowderFlo® feedstock is unique and research studies have been carried out that focused on the sintering, shrinkage, densification, microstructural evolution, effects of residual carbon content (Wu, et al. 2002a; Kwon, et al. 2004; Wu, et al. 2002b). A study on the injection molding stage, including filling and packing, has been conducted by Ilinca and co-workers (Ilinca, et al. 2000a; Ilinca, et al. 2000b; Ilinca, et al. 2002a), which

focused on various flow patterns. A three-dimensional transient finite element method was developed and used to predict uniform (axisymmetric) and nonuniform (nonaxisymmetric) filling patterns in a thick-walled cavity (M-shaped) with a diaphragm gate. The simulation of PowderFlo® feedstock (stainless steel powder with aqueous agar-gel binder) during the injection stage exhibited several flow patterns, for example: initial annular free surface flow, bypass and folding flow to form internal weld lines, and the transition from uniform to nonuniform flow with increasing filling time. The effects of inertia, yield stress, and wall slip on the filling patterns were studied to improve the MIM mold design. Further, a rectangular plate cavity (225 mm × 25 mm) with adjustable thickness (3, 4, and 5 mm) was designed and used to investigate the dynamics of filling and packing (Stevenson et al. 2001; Ilinca et al. 2002b). With an increase in filling time, the pressure profiles are compared which helped to decide the minimum packing time. The thermally induced flow instability in MIM process was studied (Stevenson et al., 2003; 2006) and two concepts were proposed: dimensionless Graetz number (Gz, ratio of heat conduction time to fill time); and a dimensionless ratio (B) indicating the sensitivity of viscosity to temperature differences in the mold. The mass flow can be separated into stable and unstable regions based on Gz and B values, which are determined by material properties, operating conditions and flow geometry. In principle, flow at low Gz and high B values conditions is unstable or asymmetrical and vice versa.

Another new development of water-soluble binders is the usage of inulin-based gel (from asphodel powder) (Yousefi, et al. 2006). In this paper, the maximal final density obtained from the feedstock (inulin-based gel binder and copper powders) via

compression molding was 91% of theoretical density, while generally the density of sintered MIM parts is more than 95% of the theoretical maximum.

Table 2.2 Comparison between PowderFlo® and conventional MIM binder (Wick, et al., 2003)

Conventional MIM binder vs. PowderFlo®		
Property	Conventional binder	Agar-based binder
Binder content	10 to 20 wt%	1.5 to 2.5 wt %
Debinding times	Many hours/day	Air-dry -- no separate debinding needed
Special operations	May include extra steps such as powder pack and solvent extraction	Water fluidizing agent evaporates after molding leaving intergranular pores open
Part thickness range	Less than 0.25 in., brittle as molded	No limitations, stiff--but elastic as-molded part
Typical tolerance control	±0.3%	±0.3%
Environmental concerns	May be explosive or toxic outgas or solvent requiring disposal	No environmental concerns

Supercritical extraction has been developed and adopted as a commonly used debinding method because a supercritical fluid has density of a liquid and low viscosity

similar to a gas. Because carbon dioxide can be easily converted into a supercritical state at relatively low temperature and low pressure, while it is relatively safe to use, it is widely used in supercritical extraction. Shimizu et al. (1998, 2001) studied the fabrication of both micro-parts and large size parts by MIM using supercritical carbon dioxide debinding method. Both studies showed this method efficient, safe and able to produce either micro or large parts. Another successful example was presented by Chartier et al. (1995). The green part (86 wt% alumina + 12 wt% paraffin oil + 2 wt% polystyrene) was extracted using supercritical CO_2 at a pressure of 30 MPa and temperature of 120°C. Compared with thermal and other debinding methods, the debinding time of supercritical extraction can be significantly reduced depending on the solvent. Rei et al. (2002) compared the results of two debinding methods: solvent (heptane) debinding and supercritical CO_2 extraction from the same feedstock molded parts. The results indicated that the solvent debinding exhibited better microstructure while the supercritical debinding exhibited better external appearance and a shorter debinding time.

A new binder for MIM was proposed by Li et al. (2003) mixing with the Fe-2Ni metal powders, which consist of wax, oil and polyethylene taking advantages of both wax-based and oil-based binder. The addition of oil reduced the green strength and maximum powders loading, but it also decreased the mixing torque and increased the debinding rate greatly which could be up to 2 mm/hr and drying time less than 20 minutes for a 6 mm-thick-part. Omar et al. (2003) compared solvent extraction with water leaching and explored the possibility of rapid debinding rate, which should avoid the tendency of the part to slump or distort during debinding. The two-step debinding

process had been introduced and two binder systems were compared. The binder consisted of paraffin wax, polyethylene and stearic acid and the part was immersed in heptane, while the second binder system consisted of polyethylene glycol (PEG) and polymethyl methacrylate (PMMA) with the part immersed in distilled water. These two binder systems were heated to remove the remaining binder. The experimental results of both solvent and water debinding did not show swelling or distortion, and performed well during handling prior to sintering stage. The heating rate from 3 to 15 °C/min in thermal debinding step was found to be successful.

2.4 Simulation of Debinding

A complete metal injection molding cycle includes feedstock mixing, injection filling and packing, debinding, and sintering. Most published papers are associated with injection molding (mold filling and packing) and sintering, but relatively little has been done on modeling debinding. Since this project is focused on debinding, the simulations of injection molding and sintering are not discussed in this section although they are very useful in practice.

Barriere et al. (2002) developed a 3D software to perform process simulation. One specialty of this simulation model was that a bi-phasic model was proposed to describe the flow of metallic powder and polymeric binder so that the segregation zones can be predicted accurately. The multi-cavity mold that was used allowed the validation and improvement of mold design and parameter for the injection molding stage of MIM process. Further, Barriere et al. (2003) discussed the determination of optimal debinding

and sintering parameter as well as the injection stage without defects and with required mechanical properties based on the 3D software mentioned above.

The concept of critical thickness was proposed by Li et al. (2003) and an equation was deduced through the analysis of debinding kinetics at which the kinetic controlling step during debinding transforms from liquid diffusion control to vapor transportation control. According to the equation, with an increase of the critical thickness, the temperature can be increased rapidly during the initial stage of debinding and vice versa. Therefore a relatively large critical thickness meant possibly faster binder removal. The equation showed the critical thickness was proportional to particle size and inversely proportional to both holding temperature and powders loading. However, this critical thickness concept was criticized by Adames and Leonov (2006), because once the part thickness reached the critical point, debinding was controlled by both dissolution and diffusion, and not only controlled by diffusion. Tsai and Chen (1995) reported that the effective diffusivity is proportional to the leaching temperature and inversely proportional to viscosity. The diffusion-controlled kinetic during binder burnout was also adopted by Shi et al. (2002) and a simulation model was proposed that can predict the remaining binder and the total burnout time under various compact shapes and processing parameters. In the paper of Adames and Leonov (2006), the experiments were conducted by using a specifically-designed device, which is able to eliminate external transport effects, to study the water debinding kinetics. It was found that the diffusivity depends on part geometry and debinding time.

Pichot (2003) proposed a solvent debinding simulation model, which was based on a second order diffusion problem with one fixed and one moving boundary. This model was validated in 1D cylinder shape part with experiment data and also able to predict when the debinding should stop and begin the presintering. Solvent debinding was investigated (Lin and Hwang, 1998) by using a specifically designed laser dilatometer to measure the in-situ dimensional changes. The total linear expansion was observed range from 0.5-2%. The dimensional alteration increased with temperature and the amount of the insoluble polymer backbone, while decreased with the molecular weight of the solvent. Thus provides a good reference to design the binder system and decide the solvent debinding condition.

Thermal debinding was studied by Ying et al. (2001) focusing on mass transfer, and a two-dimensional simulation model was established. In this paper, the polymer removal process was divided into three periods of time and each of them was explained well by this model. During thermal debinding, polymer removal was controlled by liquid flow which was affected by pressure-forced flow rather than capillary-driven flow. Further, a simulation model (Ying et al., 2004) of thermal debinding was proposed considering heat transfer, polymer pyrolysis, mass transfer, particle packing, strain and stress, equivalent stress, and their interaction. Based on this model, the defects can be attributed to the large gradient of liquid polymer saturation which results in stress gradient in different regions of the compact.

2.5 Summary

The four steps of the metal injection molding process were described with emphasis on various debinding methods. Common categories of binder recipes and consequent debinding approaches were discussed. Attention has been drawn into the aqueous agar-gel binder system for injection molding and sintering, but not for debinding. Finally, literature on the simulation models of debinding was introduced focusing on solvent, water and thermal debinding.

The present work is focused on the debinding of stainless steel mixing with aqueous agar-gel binder system. A series of debinding experiments were conducted and will be described in Chapter 3. The results of the experiments will be discussed in Chapter 4 in order to understand the debinding mechanism and improve the process.

Chapter 3

EXPERIMENTAL WORK

In this chapter, the material used in this project is first introduced based on its composition. Two molding approaches, compression molding and injection molding, are described with the process parameters and different geometries of parts are shown. Since debinding is the main concern in this project, various debinding experimental protocols are described. The sintering cycle is introduced with emphasis in temperature and atmosphere control.

3.1 Materials

The metal injection molding material used in this work is PowderFlo® (Latitude Manufacturing Technologies) 17-4 PH compound (donated by Honeywell International, Inc. Morristown, NJ, USA). This material is a dark/metallic pellet and combined with gas atomized stainless steel 17-4 powder with an aqueous gel binder. The exact formulation is protected by patents (Falelli, et al., US Patent 5, 746, 957, 1998; Zedalis, et al., US Patent 6, 268, 412, 2001). The composition of PowderFlo® 17-4 PH is listed below as Table 3.1 and Table 3.2 (Kwon, et al., 2004).

3.2 Compression Molding

Compression molding is one of the oldest techniques for processing polymers and widely applied to make a part with simple shape, such as cylinder. In the early stage of

this project, a hydraulic Carver Press machine was use to mold samples. The molds are disc-shaped with the same diameter but different thicknesses. The geometries and dimensions of compression molded samples are shown in Fig. 3.1.

The feedstock pellets were ground into smaller particles prior to compression molding for better mold filling. Then the feedstock was placed into the disc mold with excess material. Two Teflon sheets were placed between the top and bottom surfaces of the mold to obtain a smoother surface. After a defined force was applied for a specific time, the disc together with the sample was taken out and air cooled in ambient conditions. After cooling, the part was ejected from the mold. The compression molding conditions (force, temperature and dwell time) are list in Table 3.3 for three different thickness parts. The compression molded parts were placed into a sealed container ready for next debinding step.

Table 3.1 Chemical Composition Range of PowderFlo® 17-4 PH feedstock (MSDS)

Composition	Weight percentage %
Water	~7.4%
Iron	< 70%
Chromium	≤ 28%
Nickel	≤ 33.2%
Manganese	< 2%
Silicon	< 1%
Molybdenum	< 3%
Proprietary ingredient	< 1%

Table 3.2 Composition of Gas-Atomized 17-4 PH Stainless Steel Powder (Kwon, et al., 2004)

Fe	Balance
Cr	16.7 %
Cu	4.0 %
Ni	4.5 %
Nb+Ta	0.29 %
Mn	0.12 %
Si	0.45 %
C	0.031 %
Si	0.001 %
O	0.095 %
N	0.029 %

Table 3.3 Parameters of Compression Molding

Part	A-1	A-2	A-3
Part Thickness (mm)	4	8	12
Hydraulic Force (lb)	4000	4500	5000
Holding time (second)	50	55	60
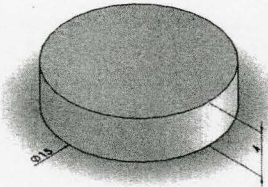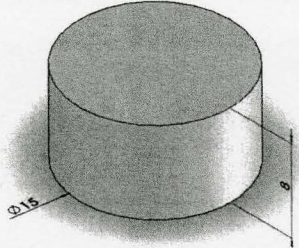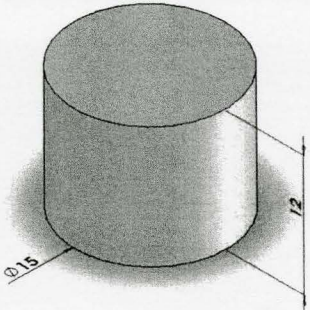
Part A-1	Part A-2	Part A-3
Thickness = 4 mm	Thickness = 8 mm	Thickness = 12 mm

Fig. 3.1 Shapes of Part A-1, A-2, and A-3 with thickness dimension and diameter = 15 mm

28

3.3 Injection Molding

An Arburg 320 S injection molding machine (55 ton clamping force) was used to make injection molded parts. With the aid of inserts, parts with adjustable thickness can be obtained in the same cavity. The geometries and dimensions of the parts are shown in Fig.3.2 and Fig. 3.3. Process parameters (temperatures, pressures and dosage) are listed in Table 3.4. Prior to and after molding this MIM feedstock, the injection machine was cleaned to ensure it was free of polymer in the screw, barrel, and nozzle area. Runners and sprue should be cleared to avoid cold materials; therefore, the materials within them should be ejected prior to each molding cycle. Once the green part was ejected, it was stored in a sealed container to keep it out of the ambient environment for debinding.

Table 3.4 Operation Parameters of Injection Molding

Temperature	Zone 1-3	82 °C
	Zone 4-5	85 °C
Pressure	Injection pressure	240 bar
Dosage	Part b-1	20 cm^3
	Part b-2	26 cm^3
	Part b-3	30 cm^3
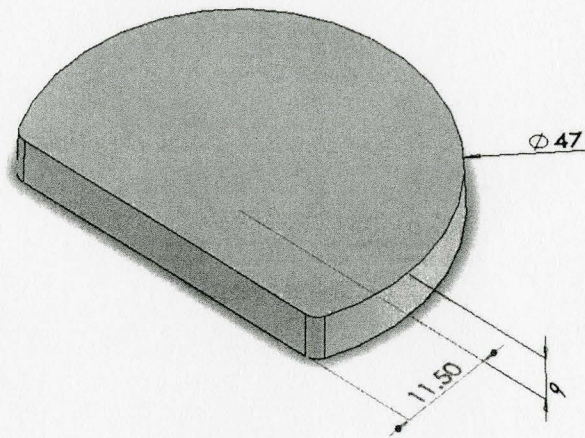
Part B-1
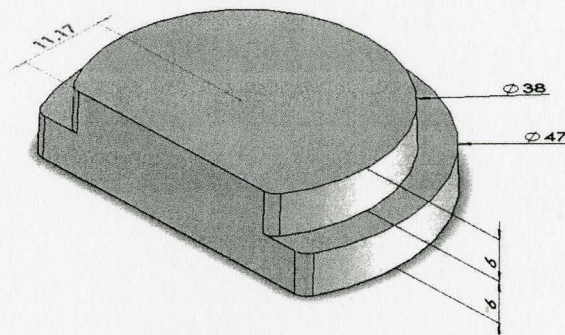
Part B-2
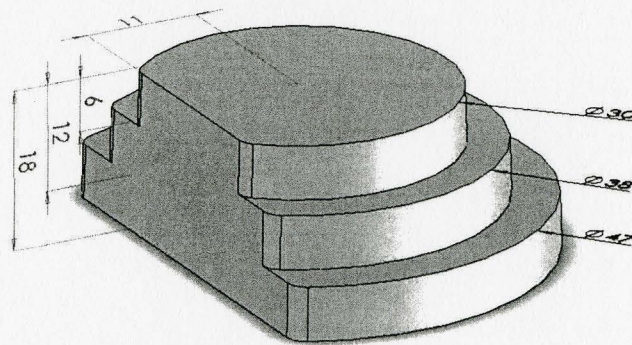
Part B-3

Fig. 3.2 Shapes of Part B-1, B-2, and B-3 with dimensions in mm
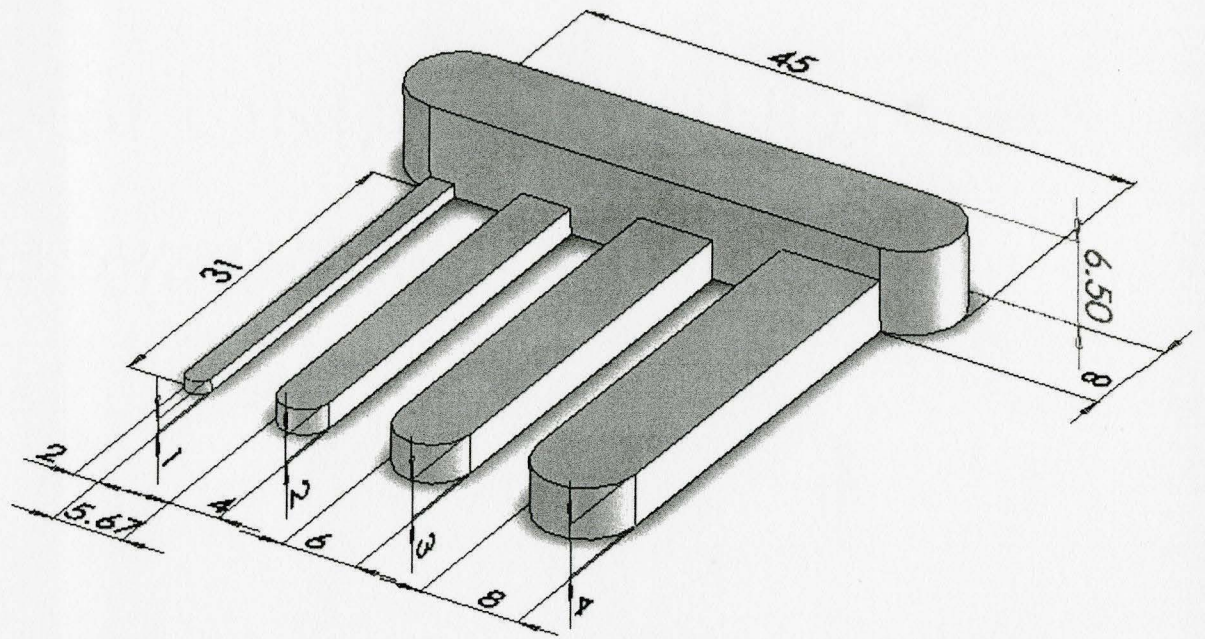
Fig. 3.3 Shape of Part C with dimension in mm

3.4 Debinding

Thermal debinding was used in this project. The green part obtained from the previous step, either compression molded or injection molded, was dried in ambient air for a certain time (t_1), and placed into PSH furnace where the part was heated from room temperature to 110°C with the designated ramp rate (r_1) and hold for a time (t_2), then the part was heated up to 275°C with the designated ramp rate (r_2) and hold for a time (t_3). Thus the thermal debinding cycle was completed and the part was taken out from the furnace. The parts were weighed and their dimensions were measured by caliper in both diameter and thickness directions before and after debinding.

There were thirty-two runs completed including four repeat runs (denoted by *) debinding experiments have been conducted for the compression molded parts and the debinding process parameters are listed in Table 3.5. Before and after the debinding experiments, the diameter of the part was measured three times in different directions. On the part surface, three points were marked by a black marker pen, i.e. one point near the center, one point near the edge, and one point in between to ensure the same spot's dimension was measured so that shrinkage in same location can be obtained.

Based on part B-1, a ¼ $2^{(5-2)}$ design was used to plan the debinding experiment to find out the effects of the five variables and ensure that no main effect was confounded with other main effects. The experimental design is shown in Table 3.6 together with the upper and lower level of the variables. For part B-2 and part B-3, the debinding process parameters are listed in Table 3.7. As to part C, three debinding experiments were conducted and the relative process parameters are summarized in Table 3.8.

32

Table 3.5 Debinding parameters of compression molded parts

Run #	t_1(hr)	r_1(°C/min)	t_2(hr)	r_2(°C/min)	t_3(hr)
1	0	10	1	10	0
2	1	10	1	10	0
3	0	10	1	10	2
4	1	10	1	10	2
29	0	2	0	2	0
30	1	2	0	2	0
31	0	2	0	2	2
32	1	2	0	2	2
33	0	6	1	6	0
34	1	6	1	6	0
35	0	6	1	6	2
36	1	6	1	6	2
17	0	2	1	6	0
18	1	2	1	6	0
19	0	2	1	6	2
20	1	2	1	6	2
25	0	2	0	6	0
26	1	2	0	6	0
27	0	2	0	6	2
28	1	2	0	6	2
9	0	6	0	6	0
11	0	6	0	6	2
13	0	6	0	2	0
15	0	6	0	2	2
21*1	0	2	1	2	0
21*2	0	2	1	2	0
23*1	0	2	1	2	2
23*2	0	2	1	2	2
5*1	0	6	1	2	0
5*2	0	6	1	2	0
7*1	0	6	1	2	2
7*2	0	6	1	2	2

Table 3.6 Debinding parameters for Part B-1

¼ 2 $^{(5-2)}$	t_1(hr)	r_1(°C/min)	t_2(hr)	r_2(°C/min)	t_3(hr)
(+) Level	1.5	1.5	1	3	1.6
(-) Level	0.5	0.75	0.5	1.5	0.8
Run #					
1	1.5	0.75	1	1.5	1.6
2	0.5	0.75	1	3	1.6
3	1.5	1.5	1	3	0.8
4	0.5	1.5	1	1.5	0.8
5	1.5	0.75	0.5	3	0.8
6	0.5	0.75	0.5	1.5	0.8
7	1.5	1.5	0.5	1.5	1.6
8	0.5	1.5	0.5	3	1.6

Table 3.7 Debinding parameters for Parts B-2 and B-3

Run #	t_1(hr)	r_1(°C/min)	t_2(hr)	r_2(°C/min)	t_3(hr)
1	4	0.5	1	1	2
1*	4	0.5	1	1	2
1**	4	0.5	1	1	2
2	4	0.5	1	1	0
3	2	0.5	1	1	2
3*	2	0.5	1	1	2
4	2	0.5	1	1	0
5	4	0.5	0	1	2
6	4	0.5	0	1	0
7	2	0.5	0	1	2
8	2	0.5	0	1	0
9	2	0.5	1	2	2
10	2	1	1	1	2
11	2	1	1	2	2

Table 3.8 Debinding Parameters for Part C

Run	t_1 (hr)	r_1 (°C/min)	t_2 (hr)	r_2 (°C/min)	t_3 (hr)
1	0	10	0	10	0
2	1	6	0	6	0
3	0.5	4	0	6	1

3.5 Sintering

The sintering experiments were conducted in the PYROX furnace where the samples to be heated should be placed in a vertical alumina tube. The heating elements of the furnace are located in the middle region around the tube. Therefore a supporting frame with layers to hold the samples is needed if more than one part is heated at one time. Alumina is a feasible material to make the frame, since it is able to undergo the temperature up to 1350°C required for the sintering of stainless steel and does not react with it.

In order to make an alumina supporting frame, an alumina tube was cut into half and 6 holes were drilled on it. An alumina rod was glued with an alumina disc beneath and then was glued into the hole on the tube while the disc should be kept vertical to the frame. The cohesive Ceramabond 813A (Aremco products, Inc. NY, USA) was used because it is applicable to ceramic-ceramic bonding and is able to undergo a temperature up to 1600°C. Thus a supporting frame with 6 layers was made. It is important that the layers are located within the heating zone to avoid a large temperature gradient.

At the beginning of the sintering, the debound parts were placed on the layers separately. The furnace was heated with a ramp rate of 5 °C/min from room temperature

to 1010 °C and held for one hour. Then the sample was heated continuously to 1350°C with a ramp rate of 2°C/min and held for 1.5 hour. The samples were then cooled to room temperature naturally. During this sintering experiment, the atmosphere is a critical factor. At temperature lower than 950°C, an oxidative air environment was used. Above 950°C, vacuum was applied for 5 minutes and then the atmosphere was changed to argon to purge the impurities. When the temperature ranged between 1010 and 1350 °C, the hydrogen was applied to provide a reductive atmosphere. Finally, argon was used again during the furnace cooling down to room temperature in order to prevent oxidation of the samples.

Due to the limited times available to use the PYROX furnace, only some compression molded parts and part C were sintered. After the sintering, part dimensions, density (MD-200S Electronic Densimeter) and weight were measured.

3.6 Summary

In this chapter, the material and consequent experiments, including compression molding, injection molding, debinding, and sintering, are introduced based on different parts. In the next chapter, all the experiment results will be discussed.

Chapter 4

RESULTS AND DISCUSSION

This chapter consists of three sections. In first section, debinding results of injection molded parts are discussed, focusing on the influence of debinding process parameters, thickness and thickness transition. The effect of thickness and debinding time of compression molded parts are studied with an emphasis on apparent performance. Sintering results such as final density of selective parts are compared.

4.1 Injection molded parts

The debinding study of injection molded parts is the main focus in this section. Eight runs of debinding experiments for Part B-1 were conducted to set up three linear regression models and investigate the effects of debinding process parameters on debinding results such as binder removal and dimensional shrinkage (two directions). Since the effect of thickness is the most important factors in determining the debinding schedule, further debinding experiments for Part B-2 and B-3 were conducted in order to find out a time efficient manner with respect to thickness.

Debinding results involve polymer removal (wt %), thickness shrinkage (H %) and diameter shrinkage (D %). These debinding results are ratios of difference after debinding to original values so that they are dimensionless. In this chapter, diameter shrinkage refers to the dimensional change in the direction vertical to the flat side (see Fig. 3.2). The factors studied consist of holding time at room temperature (t_1), heating

rate from room temperature to 110°C (r_1), holding time at 110°C (t_2), heating rate from 110 to 275°C (r_2), and holding time at 275°C (t_3). The specific temperatures of 110 and 275°C were chosen is because the feedstock shows a noticeable weight loss at around 100 and 270°C when it is heated up at the ramp rate of 2.5°C/minm from room temperature to 300°C. The temperatures of 110 and 275°C are also recommended by the manufacturer.

4.1.1 DOE for Part B-1

Design of Experiments (DOE) is a common method to plan experiments in a way that helps to maximize the information and reduce the number of necessary experimental runs. Compared with a full design of experiments, fractional factorial design is more often used since it can reduce the number of experimental runs required. For example, a ¼ 2^5 design can ensure that no main effect is confounded with other main effects, but the main effects are confounded with two factor interaction(s).

Debinding results of Part B-1 are applied to set up linear regression models to determine the significance of process variables affecting polymer removal (wt %), thickness shrinkage (H %) and diameter shrinkage (D %). Based on the literature (Loh and German 1996), the two factor interactions or higher order interaction terms during debinding are small compared with main effects and it is reasonable to neglect them. So a $2^{(5-2)}$ design is chosen. Therefore eight debinding experimental runs are decided. The debinding process variables, with coded levels, of Part B-1 are listed in Table 4.1. The screening designs in coded levels and consequent results are summarized in Table 4.2.

The calculation of coefficient (main effects confounded with two factor interactions) can be seen in Appendix A and the results are shown in Table 4.3.

Since the two factor interactions or higher order interactions are negligible, the coefficient can be considered equivalent to main effects of the factors.

Table 4.1 Debinding process parameters with codes for Part B-1

Process Variables			Coded levels	
			-	+
x_1	t_1 (hr)	Holding time at room temperature (RT)	0.5	1.5
x_2	r_1 (°C/min)	Heating rate from RT to 110°C	0.75	1.5
x_3	t_2 (hr)	Holding time at 110 °C	0.5	1
x_4	r_2 (°C/min)	Heating rate from 110 to 275 °C	1.5	3
x_5	t_3 (hr)	Holding time at 275 °C	0.8	1.6

Table 4.2 Debinding variables and results of Part B-1

Run #	t_1 (hr)	r_1 (°C/min)	t_2 (hr)	r_2 (°C/min)	t_3 (hr)	total time (hr)	wt % (%)	H% (%)	D% (%)
1	+	-	+	-	+	7.889	9.11	0.92	1.4
2	-	-	+	+	+	5.972	9.1	0.99	1.26
3	+	+	+	+	-	5.194	8.92	0.98	1.46
4	-	+	+	-	-	5.111	8.85	2.14	0.942
5	+	-	-	+	-	5.641	9.11	1.09	0.71
6	-	-	-	-	-	5.589	8.96	0.33	1.17
7	+	+	-	-	+	6.494	9.01	0.38	1.15
7*	+	+	-	-	+	6.494	8.93	0.66	1.18
7avg	+	+	-	-	+	6.494	8.97	0.52	1.165
8	-	+	-	+	+	4.494	8.7	1.08	0.37
9	1	1.5	0.5	3	1	4.394	8.86	1.09	0.458

(* denotes repeating experiment, 7avg denotes average values of 7 and 7*)

Table 4.3 Coefficients of linear regression models

Coefficient	l_0 average	l_1 (1+45)	l_2 (2+35)	l_3 (3+25)	l_4 (4+15)	l_5 (5+23+14)
		t_1	r_1	t_2	r_2	t_3
wt%	8.965	0.0625	-0.105	0.03	-0.0075	0.005
H%	1.006	-0.129	0.174	0.251	0.0287	-0.129
D%	1.0596	0.124	-0.0754	0.206	-0.110	-0.0109

4.1.1.1 Effect of process parameters on binder removal

The weight loss of compact during thermal debinding directly reflects the progress of the binder removal process. In debinding a product made of PowderFlo® feedstock, weight loss is due to water removal and polymer removal from the internal part of the compact to the outer surface.

In the debinding step, when the temperature gradually increases, water evaporates, agar starts to melt at around 85°C and then polymer decomposes. Thus the overall removal of binder is a complicated combination of evaporation, liquid and gas migration, and pyrolysis of polymer in the porous structure. The binder removal is mainly dominated by pressure-driven liquid flow.

As can be seen from Table 4.3, the weight loss percentage (wt %) of Part B-1 during debinding increases with an increase in three holding periods, i.e. room temperature (RT), 110°C and 275°C; in contrast, when increases the two heating rates, the weight loss percentage decreases. In the following, the influences of five variables will be discussed based on Part B-1.

4.1.1.1.1 Effects of holding times

Although water evaporates and reduces during injection molding, a significant amount of water remains in the compact. Since the water content of feedstock is initially around 7.5 wt%, the water content of the molded part can be assumed to range from 6.5 to 7.5 wt%. In this present project, for convenient purpose, the room temperature is consistently taken as 22°C and the relative humidity as 60 % in ambient atmosphere. Thus the saturation water vapor pressure can be obtained by calculation as 2629 Pa[3] in ambient air. The water vapor concentration in air is 0.00978kg/kg dry air[4]. Thus the water concentration within the compact is much higher than ambient atmosphere. The increase in temperature, and subsequently the vapor pressure causes a slight pressure gradient between the internal compact and the outer surface that helps for diffusion of water to air. This is a convenient, low cost, but time consuming way for water removal because the pressure difference between the internal and ambient atmosphere is very limited and the slow drying rate does not arise defects. So extending the air-drying time facilitates water

---

[3] Saturation vapor pressure: $P_s = 610.78*\exp(t/(t+238.3)*17.2694)$ (unit: Pa), where t is temperature in °C.

[4] kg water vapor / kg dry air $= 0.62*10^{-5}*P$, where P is actual vapor pressure in Pa.

removal and consequently results in higher weight loss during debinding. Furthermore, any actions that may enhance the air flow and provide drier air may also enhance the water removal from the compact.

When a compact is held at 110°C, the pressure inside the compact is much higher than outside the compact due to residual water converting into vapour at a higher temperature. Similarly, the saturation water vapor pressure as $1.43*10^5$ Pa can be obtained by calculation via the same equation shown as footnote (2). This pressure gradient is much higher than in the previous air-drying period. Thus increasing the holding time at 110°C may enhance the residual water to evaporate and diffuse to outer surface, which enhance the water removal and weight loss.

When a compact is held for a period of time at 275°C, there is still significant amount of polymer residue inside the compact. The polymer liquid removal becomes slower because polymer liquid saturation declines with time, and the polymer vapor has to diffuse to outer surface via the porous medium. So increasing the holding time at 275°C can also facilitate the residue polymer removal that results in higher weight loss.

Although the three holding times all can enhance binder removal, they have different significance effects. As can be seen from Table 4.3, fits of t_1 and t_2 are larger than the fit of t_3. This can be explained by the difference in content of water and polymer originally in the feedstock. Since approximately the water content is 7.5 wt% and the polymer content is 1.5wt%. Therefore the fits of holding times show an accord with the water and polymer changes in weight during debinding.

4.1.1.1.2 Effects of heating rates

During debinding water and polymer should ideally diffuse from the internals of the part to the outer surface in the shortest time while preventing defects. But higher heating rates increase the opportunity of defects forming (e.g. voids, cracks), especially the initial heating rate (r_1), i.e. the heating rate from room temperature to 110°C.

The defects occurrence can be explained by using the criterion of bubble formation. The bubble formation depends on whether the equilibrium vapours pressure is higher than the ambient pressure. But if the equilibrium vapor pressure surpasses a critical pressure, the bubble breaks. Likewise, the saturation water vapor pressure is proportional to $\exp(t/(t+238.3))$ (herein t refers to temperature in °C). For example the saturation water vapor pressure is 143 kPa at 110°C and 2.63 kPa at 22°C. It can be seen that when the compact is heated up, the internal vapor pressure increases dramatically. Since the polymer still remains relatively rigid in low temperature, i.e. the initial heating period, internal pressure may develop and cause cracking if the diffusion rate of water vapor is slower than the water vapor formation rate. Therefore too fast heating may result in fast bubbles forming and then bubble breaking. The initial heating rate should be kept reasonably slow to prevent defects from occurring.

Generally, a large void is easier to form in the core region than in surface area because of the pressure drop across the porous medium. When more and more voids form and accumulate in the core region, the swelling-like defect can be observed. If these internal large voids are connected to the surface area, it becomes visible cracking. When the water removal is completed, tortuous channels form, which make it easier for the

consequent polymer extraction. Thus the heating rate can be accelerated in the polymer removal stage.

From Table 4.3, the data shows that both heating rates have negative effects on weight loss, which means that an increase in both heating rates may prohibit the binder removal. This agrees with the experimental results. Comparing with the fits of the five variables, the initial heating rate is the most significant factor in binder removal, which is also in accord with the previous research results.

4.1.1.2 Effects of process parameters on shrinkage

Because shape of Part B-1 is equivalent to a large portion of a cylinder with 47mm-diameter and 6mm-thickness, the binder extraction varies in different directions that result in various shrinking performance.

The binder removal process can be considered as a mass flux that includes liquid and vapor flux. Although the total binder mass flux is nonuniform, binder mass flux is easier to flow toward the short distance than long distance. The stress distribution is steeper toward the thickness direction than toward the diameter direction.

As can be seen from Table 4.3, compared with other variables, the holding time at 110°C is the most significant factor on shrinkages in both directions and the holding time at RT is the second significant factor. The shrinkage occurs when the binder is removed. PowderFlo® feedstock has an initial water content as approximately 7.5 wt%, which is approximately equivalent to 36 vol% at room temperature. The large volume content of water is the main reason for shrinkage. The holding times at 110°C and RT are the most

45

significant factors on water removal, as a result, also the most significant factors on shrinkage. With all the water left the compact, it comes with volume change and the porous internal structure forms. In contrast, an increase of holding time at 275°C can reduce shrinkages in both directions. It seems that the internal voids redistribution happens during holding at 275°C, which makes small change in volume.

According to the statistical model in Table 4.3, an acceleration of both heating rates is able to increase the thickness shrinkage but reduce the direction shrinkage. This is due to the fact that the equivalent stress distribution differs in directions within the compact. Inside the compact there are pores filled with water and polymer vapor that apply stresses on the liquid and solid state materials. Comparing the dimension of thickness (6mm) and diameter (47mm) of Part B-1, binder diffusion requires less time towards the thickness direction than towards the diameter direction. So there is relatively higher shrinkage in the thickness direction due to the smaller initial thickness dimension.

4.1.1.3 Effect on total debinding time

The cost of production is associated with efficiency so the total debinding time is a significant portion of cost in metal injection molding. As shown in Table 4.2, the total debinding time for run #9 requires 3.39 hour furnace heating plus one hour air-drying which is the shortest cycle of all and the debound part is free of defects. Therefore, from the industrial point of view, run #9 is the best option to debind Part B-1 in all nine debinding experiments.

In regards to production cost, if the debinding time is not a concern in the production, it is suggested to prolong the air-drying time which makes it possible to accelerate the consequent heating rates and reduce the furnace dwelling periods, thus results in lower production cost; if the debinding time is a large concern, it is suggested to cancel the air-drying step and forward to furnace heating directly. Both ways have been approved to be able to debind a part free of defect.

4.1.2 Effect of thickness

The thickness factor is the main concern in the present project. In this section, the debinding study will focus on Parts B-2 and B-3. The objective is to explore the effects of debinding process variables on overall debinding and determine a time-efficient schedule with respect to part thickness without defects.

In the following discussion, same run number refers to the same debinding process parameters for both Part B-2 and B-3. The parameters as well as the results are listed in Table 4.4 for Part B-2 and Table 4.5 for Part B-3. In Figures 4.1 - 4.3 and 4.5 - 4.16, the experimental run numbers of Part B-3 are differed from Part B-2 by following "'", for example: #1 refers to run # 1 for part B-2, and #1' refers to run #1 for part B-3; in addition, the solid lines represent Part B-2 while the dash lines represent Part B-3.

The effects of each process parameter on debinding results will be discussed respectively.

Tbable 4.4 Debinding Process Parameters and Results for Part B-2

Run	t_1	r_1	t_2	r_2	t_3	wt	H	D	Total debinding time
units	(hr)	(°C/min)	(hr)	(°C/min)	(hr)	%	%	%	(hr)
1avg	4	0.5	1	1	2	8.718	1.002	0.761	12.68
2	4	0.5	1	1	0	8.554	1.238	0.640	10.68
3avg	2	0.5	1	1	2	8.906	1.908	1.037	10.68
4	2	0.5	1	1	0	8.779	1.565	0.634	8.68
5	4	0.5	0	1	2	8.968	2.068	1.293	11.68
6	4	0.5	0	1	0	8.810	1.999	1.083	9.68
7	2	0.5	0	1	2	8.924	2.103	1.033	9.68
8	2	0.5	0	1	0	8.858	2.164	1.187	7.68
9	2	0.5	1	2	2	8.718	1.597	1.047	9.308
10	2	1	1	1	2	8.462	0.869	0.757	9.22
11	2	1	1	2	2	8.411	0.873	0.598	7.84

Table 4.5 Debinding process parameters and results for Part B-3

Run	t_1	r_1	t_2	r_2	t_3	wt4%	H%	D%	Total debinding time
units	(hr)	(°C/min)	(hr)	(°C/min)	(hr)	%	%	%	(hr)
1avg	4	0.5	1	1	2	8.683	0.828	0.964	12.68
2	4	0.5	1	1	0	8.356	0.644	0.643	10.68
3avg	2	0.5	1	1	2	8.703	1.514	1.025	10.68
4	2	0.5	1	1	0	8.258	0.742	0.298	8.68
5	4	0.5	0	1	2	8.693	1.173	1.169	11.68
6	4	0.5	0	1	0	8.237	1.347	0.811	9.68
7	2	0.5	0	1	2	8.931	1.468	1.034	9.68
8	2	0.5	0	1	0	8.754	1.249	0.815	7.68
9	2	0.5	1	2	2	8.145	0.723	0.735	9.31
10	2	1	1	1	2		swelling		9.22
11	2	1	1	2	2		swelling		7.84

4.1.2.1 Effect of holding time at RT

During air-drying, water within the compact diffuses to outer layer or evaporates to outer surface. This is driven by pressure gradient between the inside and outside of the compact due to the different moisture content. This pressure difference is limiting such that it is difficult for water diffusion especially from the core region of a thick part. As shown in Fig. 4.2, and 4.3, Part B-3 shows less dimensional changes and accordingly has more dimensional stability than Part B-2. When it comes to compare the binder removal influence, except for run #6' that shows a comparatively large fluctuation, the thicker part shows less weight change and also more stable binder removal performance than the thin part B-2. Therefore it seems that holding time at room temperature is not a significant factor and extending it cannot help much for binder removal especially for a thicker part such as Part B-3 when the air-drying time ranges from 2 to 4 hours.

4.1.2.2 Effect of initial heating rate

When the initial heating rate as 0.5°C/min is used, both Part B-2 and Part B-3 have good part appearance and performance; but when it is accelerated to 1°C/min, Part B-3 shows swelling and cracking.

With an increase in temperature, the vapor pressure increased dramatically, thus the water inside the compact has a large driving force to diffuse out of the compact. Fig. 4.4 shows the representative internal composition of a MIM part. The black spots refer to metal powder particles that are surrounded by vapor or liquid binder. If the vapor or liquid binder cannot diffuse sufficiently, the pressure of the vapor might become large

enough to apply on the metal particles to give ways for mass transport. Therefore voids may be generated in the compact. Furthermore due to the non-uniform mass flow, the voids distribution is also inhomogeneous thus resulting in uneven shrinkage and poor dimensional control, which is a major disadvantage for thermal debinding since the internal stresses created become a source of defects.

For part B-2, when the initial heating rate increases from 0.5 to 1°C/min, the binder removal difference can be up to 4%. As can be seen in Fig. 4.5, the binder removal drops from 8.9 wt% (run #3) to 8.46 wt% (run #10), and it drops from 8.7 wt% (run #9) to 8.4 wt% (run #11). It seems that there is considerable binder residue still remaining within the compact. As a result, the shrinkages in both the thickness and diameter directions decrease with an acceleration of initial heating rate; in addition, the thickness direction shows bigger shrinkage than the diameter direction. As shown in Fig. 4.6 and Fig. 4.7, when the initial heating rate increases from 0.5 to 1°C/min, the H% declines from 1.6~1.9% to 0.9%, while the D% declines from 1% to 0.7%. This might be due to the binder diffusion takes shorter time towards the thickness direction. So in the thickness direction shows more shrinkage than in the diameter direction.

This indicates that initial heating rate is the most critical factor that determines the success of a debinding profile.

4.1.2.3 Effect of holding time at 110°C

The holding time at 110°C mainly aims for water removal. The thinner part B-2 has larger fluctuation than part B-3 in binder removal (if run #4'is negligible) when the

holding time at 110°C increases from 0 to 1 hour, as shown in Fig. 4.8. It is due to the thicker part is more difficult for water diffusion so that thinner part is more sensitive to this holding time. For the thinner part B-2, dwelling time at water removal stage affects the shrinkage more significantly than part B-3, particularly in the thickness direction (see Fig. 4.9). A distinct example is the thickness shrinkage reduces from 2.0% (run #5) to 1.0% (run #1) when dwelling time increases from 0 to 1 hour. As shown in Fig. 4.10, the thicker part B-3 also has declining trend in diameter shrinkage, but part B-2 has steeper declining trend. This all shows that holding time at 110°C is a more sensitive factor for thinner part. Therefore extending the dwelling time in water removal stage is beneficial to obtain more homogenous binder extraction and more precise dimensional control, particularly the thicker part requires longer holding time at 110°C for good debinding performance.

4.1.2.4 Effect of secondary heating rate

Based on Fig. 4.11, 4.12, and 4.13, for the case where secondary heating rate accelerates from 1 to 2°C/min, the thicker part B-3 has larger changes in the binder removal and shrinkages in two directions than part B-2. As can be seen from the figures, the binder removal of Part B-3 decreased from 8.7 wt% (run #3') to 8.1 wt% (run #9') when the secondary heating rate doubles to 2°C/min, while part B-2 shows less than 0.2 wt%. Similarly in shrinkages, part B-3 shows a decrease in H% from 1.5 to 0.7% and also a decrease in D% from 1.0 to 0.7%, comparatively, part B-2 shows less than 0.2% in both shrinkages. As the water removal progresses, the porosity of the part is increased. But it

is still not easy for the polymer in thicker section to diffuse out of the compact and accordingly takes longer time. The thinner part B-2 shows very stable debinding results although the secondary heating rate is doubled. This implies that the thinner part can be heated up at a faster rate after water removal.

4.1.2.5 Effect of holding time at 275°C

The holding time at 275°C is for polymer removal. The debinding results affected by this can be seen in Fig. 4.14, 4.15, and 4.16. With an increase of holding time in the polymer removal stage from 2 to 4 hour, the binder removal increases slightly for thinner part B-2 (less than 0.2% in 4 runs) while it shows greater gradient (may up to 0.5%) for the thicker part B-3. Because polymer is easier to diffuse from thinner section and probably already diffuse during the secondary heating up stage. As a result, the thinner part B-2 shows stable or slight dimensional change when extending this dwelling time compared with the thicker part B-3. The thicker part like Part B-3 is more beneficial in binder extraction and dimensional control when increasing the holding time for polymer removal. It should be noted that for thicker part sections, this holding time has more influence on the diameter shrinkage than thickness shrinkage.

In the following figures, the measurement error of mass is ±0.001 gram, while the measurement error of dimension is ±0.01 mm.
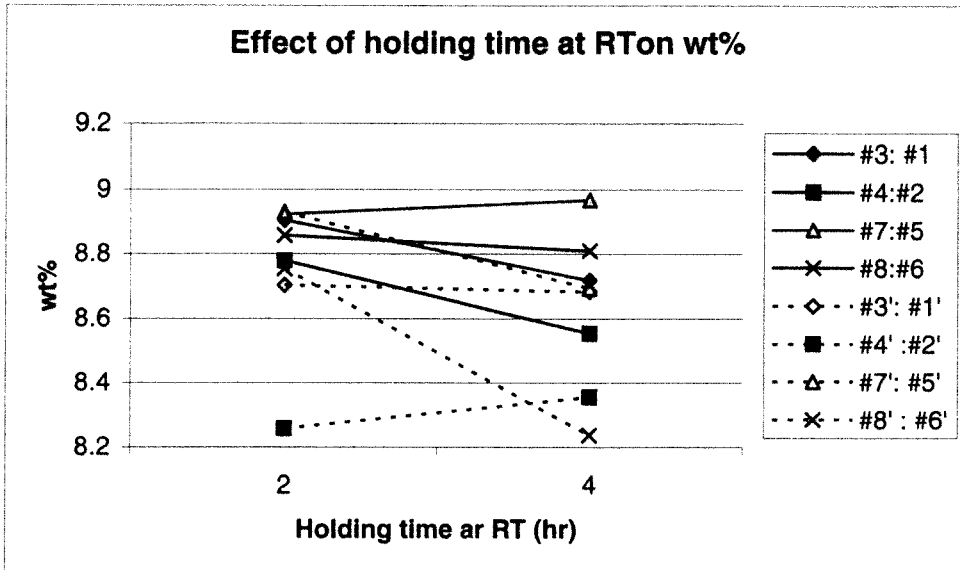
Fig. 4.1 Effect of holding time at RT on binder removal
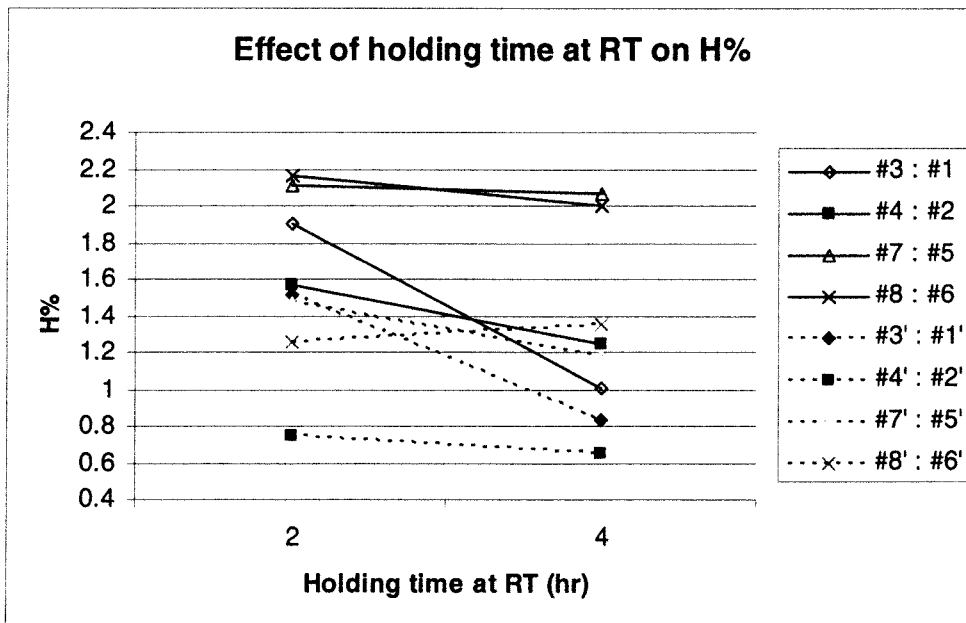
Fig. 4.2 Effect of holding time at RT on thickness shrinkage

Effect of holding time at RT on D%
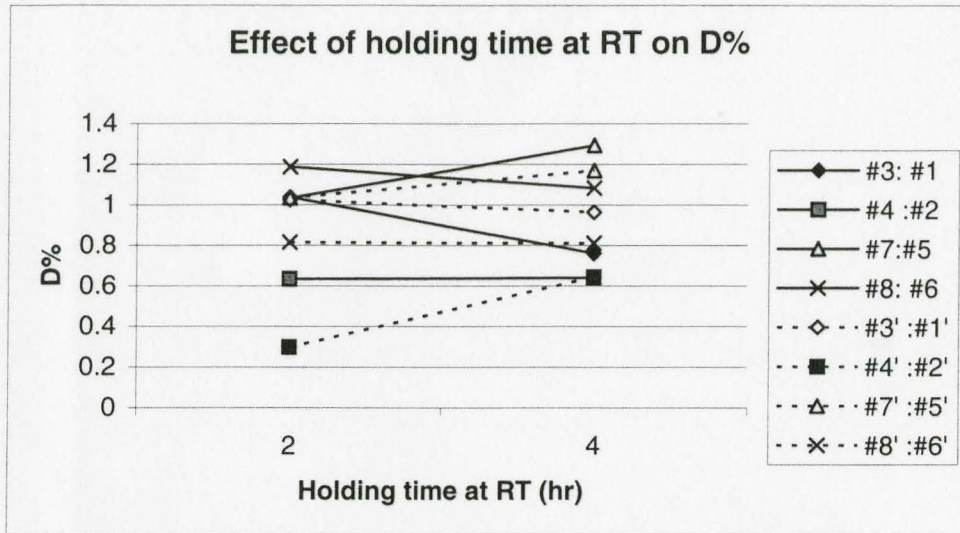
Fig. 4.3 Effect of holding time at RT on diameter shrinkage
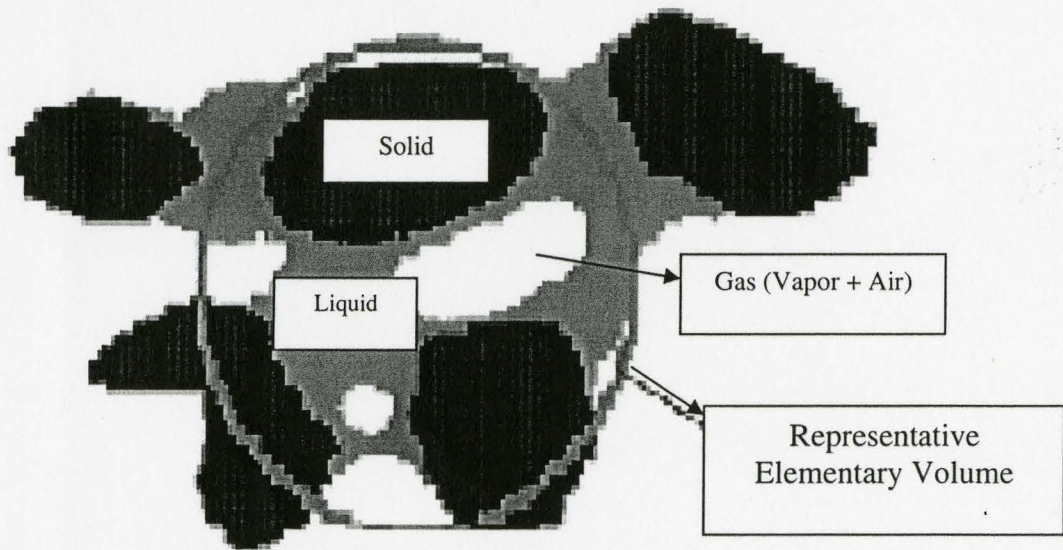
Fig. 4.4 Schematic picture of internal composition (Ying, Shengjie, et al. 2001)

Effect of initial heating rate on wt%
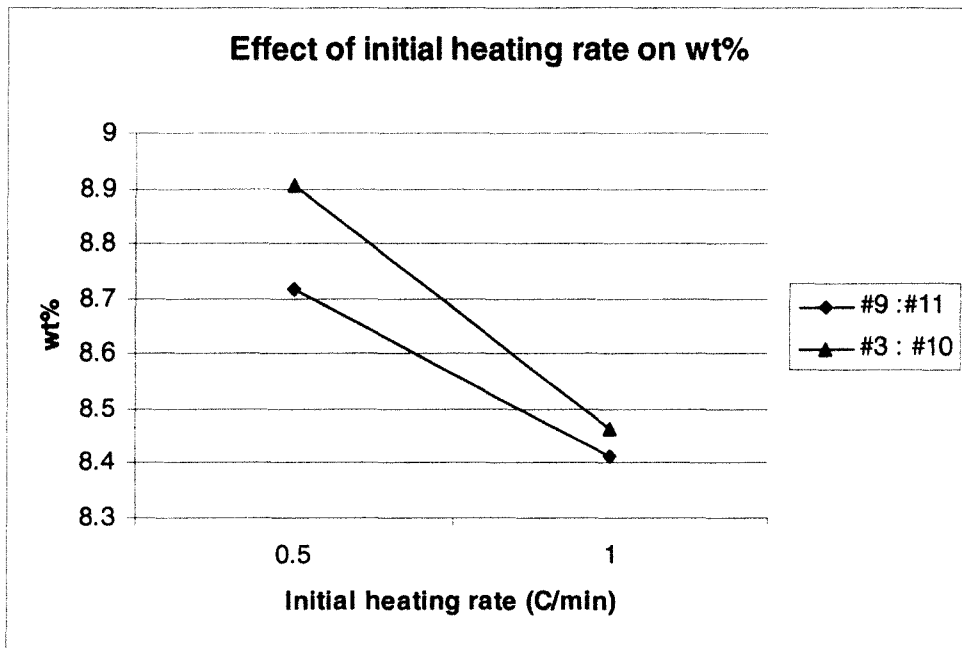
Fig. 4.5 Effect of initial heating rate on binder removal

Effect of initial heating rate on H%
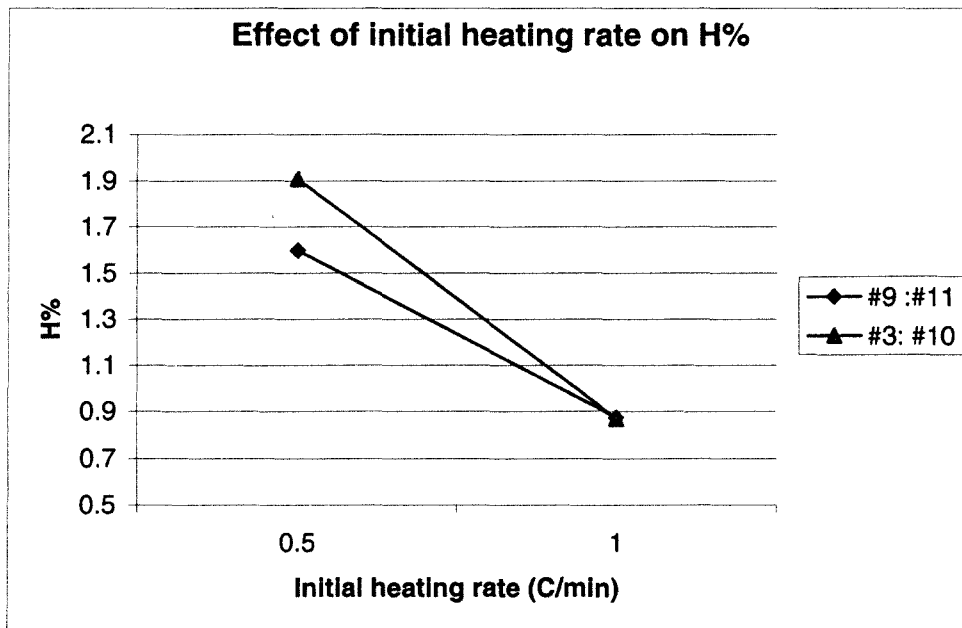
Fig. 4.6 Effect of initial heating rate on thickness shrinkage
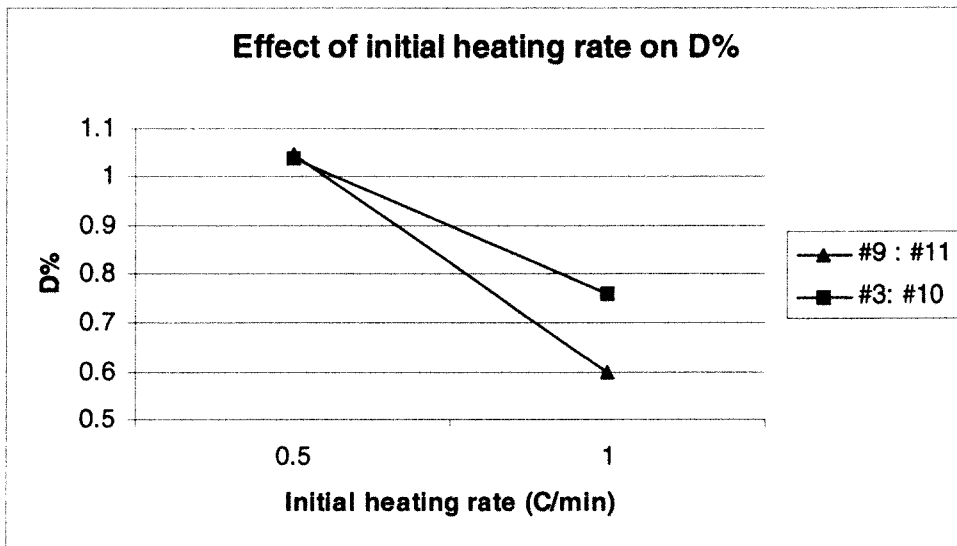
Fig. 4.7 Effect of initial heating rate on diameter shrinkage
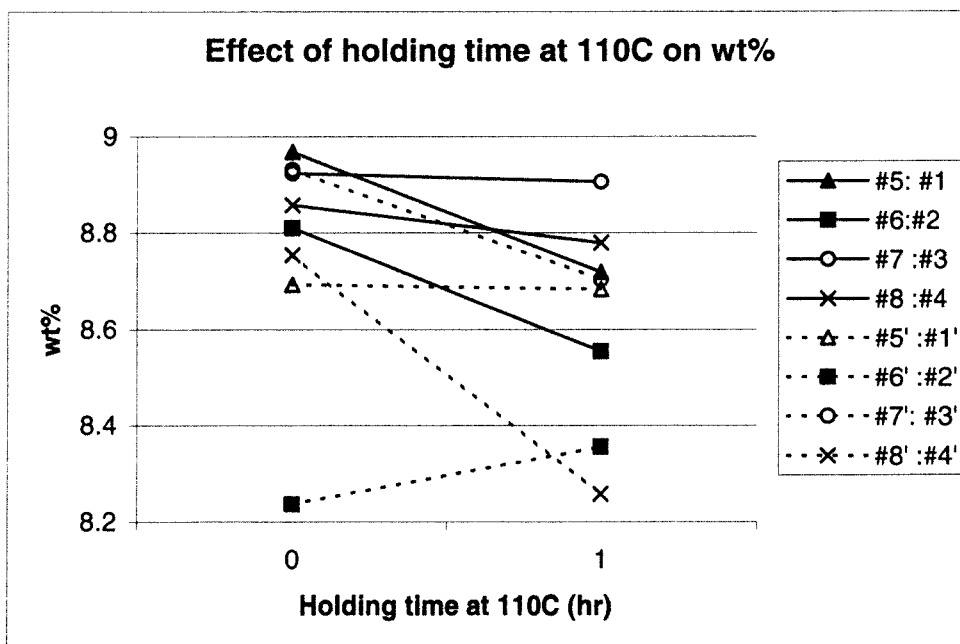
Fig. 4.8 Effect of holding time at 110°C on binder removal

Effect of holding time at 110C on H%
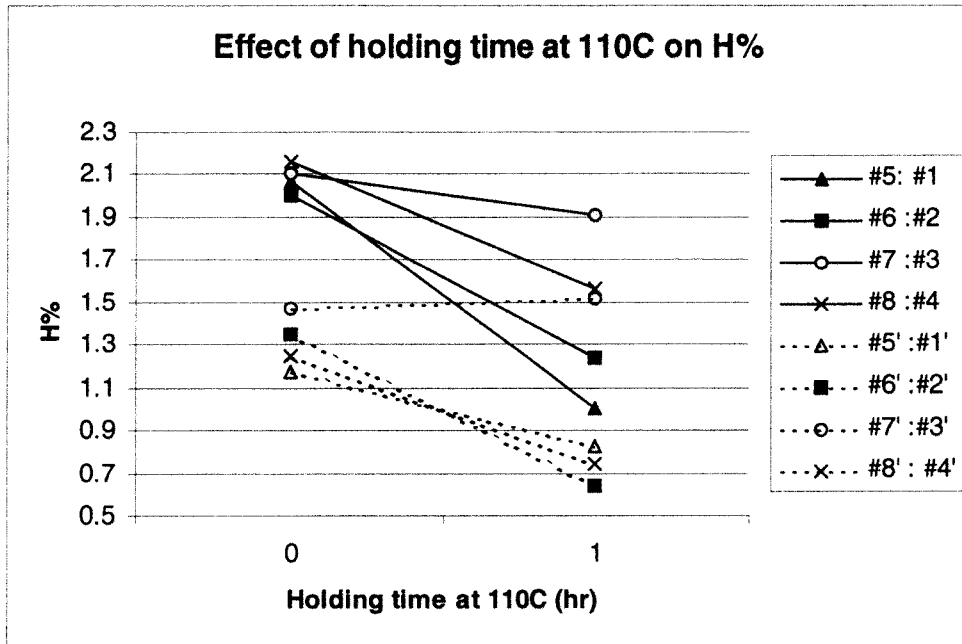
Fig. 4.9 Effect of holding time at 110°C on thickness shrinkage

Effect of holding time at 110C on D%
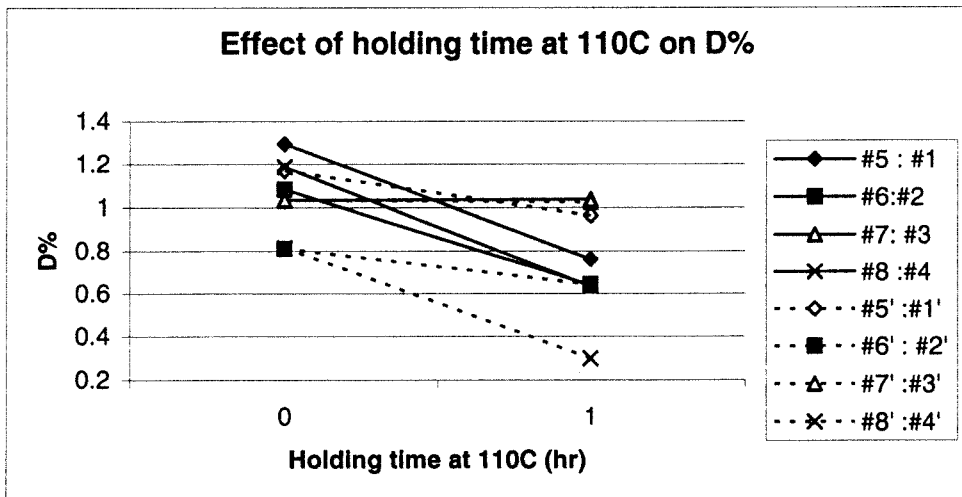
Fig. 4.10 Effect of holding time at 110°C on diameter shrinkage
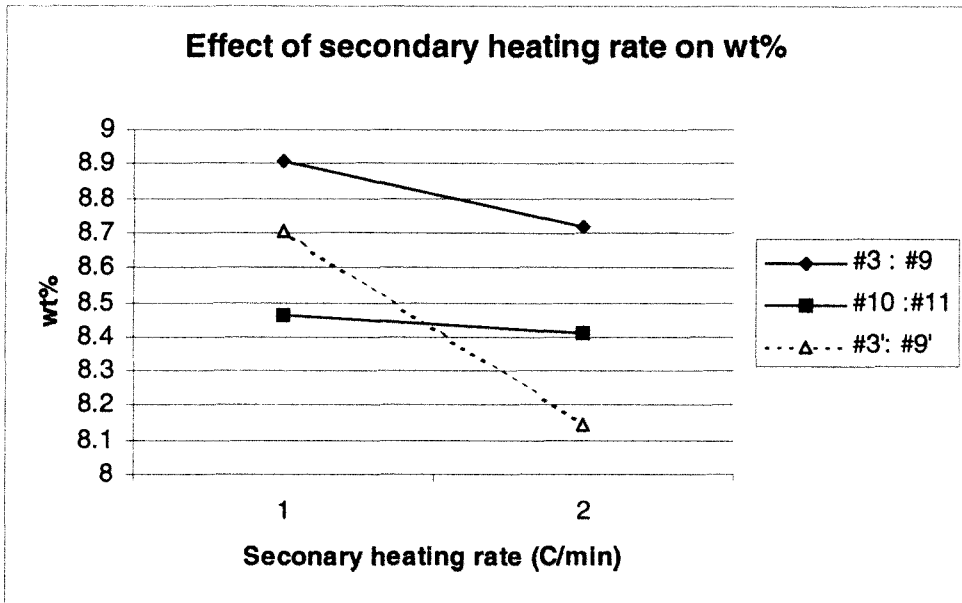
Fig. 4.11 Effect of secondary heating rate on binder removal
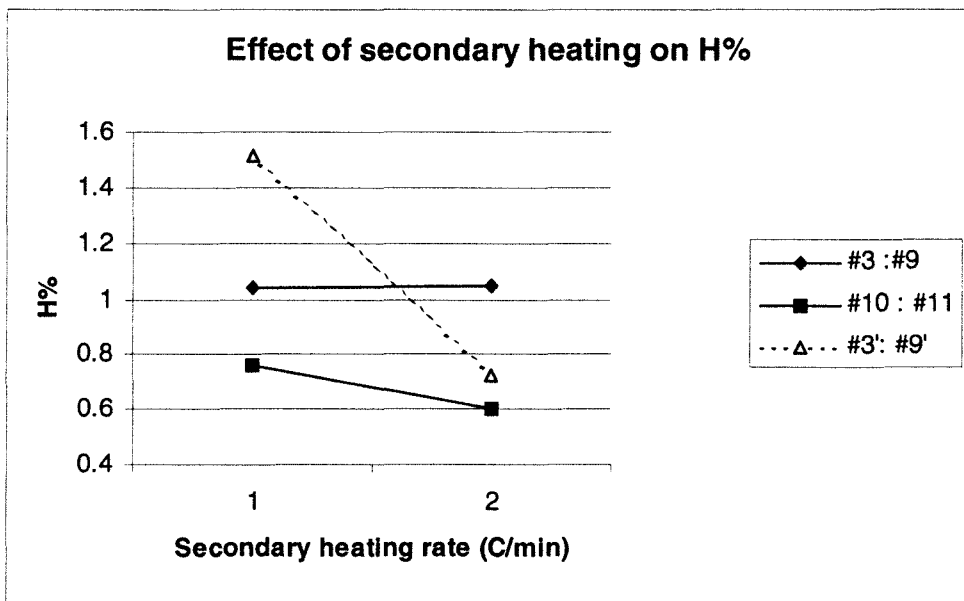
Fig. 4.12 Effect of secondary heating rate on thickness shrinkage

60
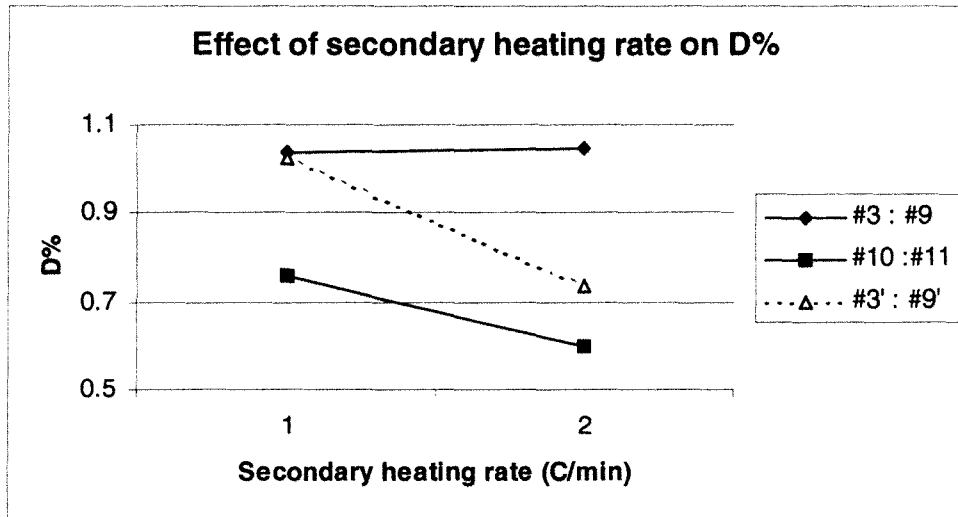
Fig. 4.13 Effect of secondary heating rate on diameter shrinkage
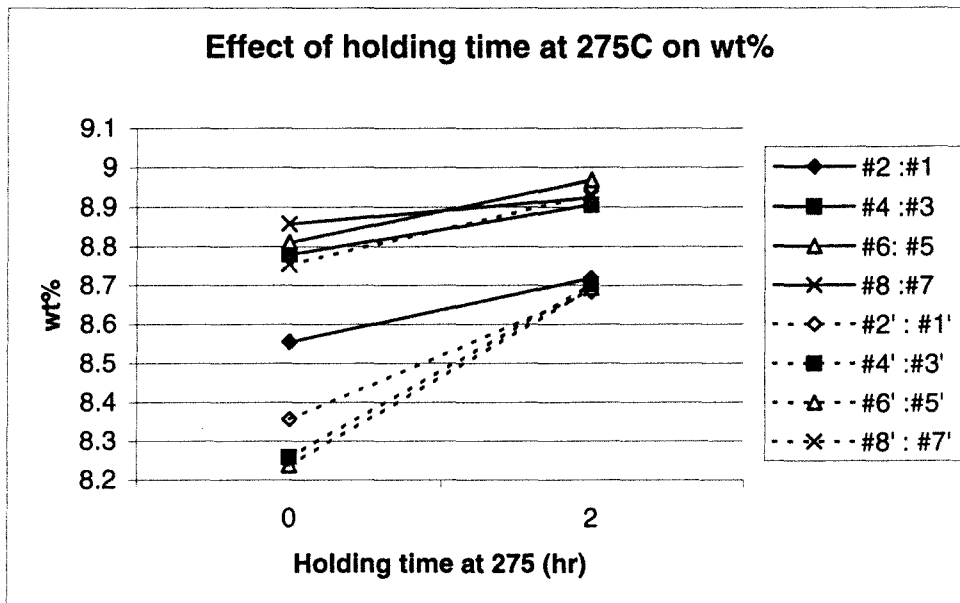
Fig. 4.14 Effect of holding time at 275°C on binder removal
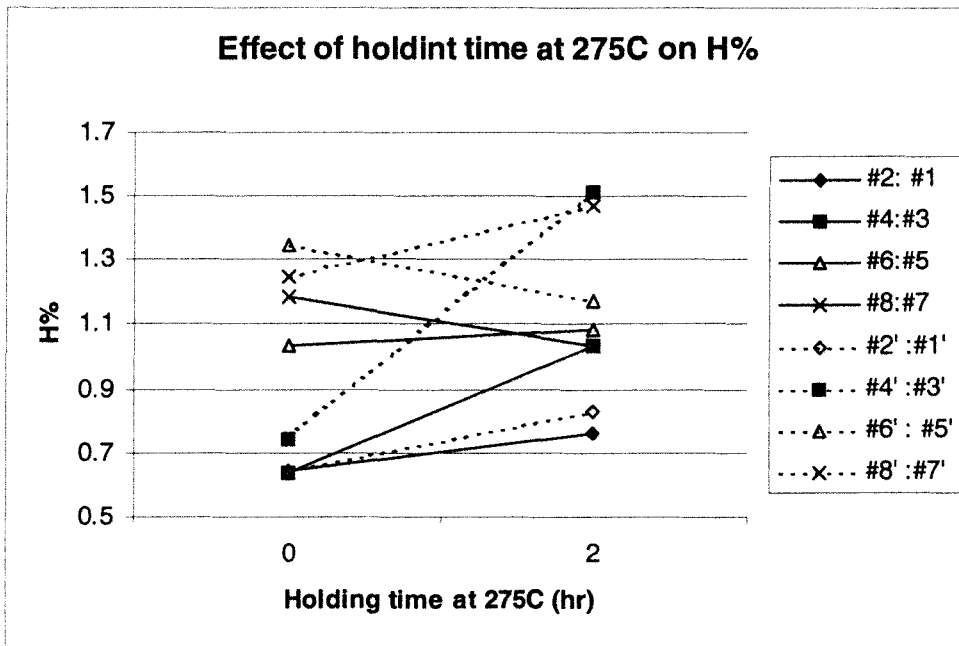
Fig. 4.15 Effect of holding time at 275°C on thickness shrinkage
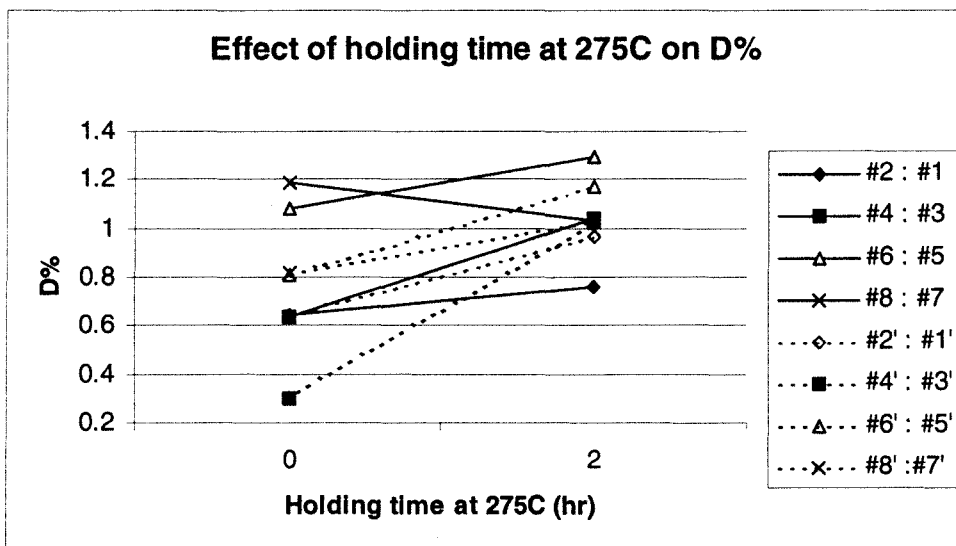
Fig. 4.16 Effect of holding time at 275°C on diameter shrinkage

4.1.3 Thickness transition discussion

In many cases a metal injection molded part may have thin and thick section(s). But the joint area between thin and thick section is a major concern because defects such as cracking occur easily in the transition section. Part C (as shown in Fig. 3.3) was designed to investigate the thickness transition. Part C is divided into five sections that are close to rectangular shape, as listed in Table 4.6 with dimensions. Consequently three debinding runs to fully debind section 1, 3, and 5 respectively are scheduled and summarized in Table 4.7.

Although the debound parts were handled carefully, cracking occurred at the joint area between sections 1 and 5. In addition, run #1 and #2 also showed swelling in central region of section 4 and 5. This indicates that a fast debinding cycle aim for full debinding of the thinnest section cannot avoid the defects generated in the thicker sections; in contrast, a slow debinding schedule aim for full debinding of the thickest section may result in insufficient handling strength within the thinner sections. Without the binders, the remaining metal particles are loosely packed together and cannot withstand any distortion. Thus cracking becomes the most common problem in this situation. It was reported that generally a compact can undergo as a maximum torque as 10^{-4} (N*m) without distortion (German and Bose, 1997). Once the compact suffers from a torque higher than the critical value, distortion occurs. Because binders diffuse preferably from thin section so that it has less binder content than the thicker section as debinding progresses. The difference in binder content also makes a difference in the thermal expansion coefficient, which creates a stress at the thin-thick joint area. The stress

develops with the difference in binder content and increasing temperature. It is noteworthy that Part C is capable to maintain its shape after water removal but fails for shape retention after polymer removal. Therefore it is advised to complete polymer removal and sintering in the same furnace without any movement.

In general, combination of too thin and too thick sections should be avoided when a part is to design. If the thin and thick sections are necessary, it is suggested to increase the joint area and provide uniform packing during molding. For PowderFlo® product, the water removal can be conducted in a low temperature furnace or just drying in ambient atmosphere, and then complete the polymer removal and sintering in the same furnace without any handling. In later experiments a sintered part C without distortion (only slightly warpage) was obtained via this method.

Table 4.6 Division sections of Part C with dimensions (unit: mm)

	length	width	thickness
Section 1	31	2	1
Section 2	31	4	2
Section 3	31	6	3
Section 4	31	8	4
Section 5	40	8	6.5

Table 4.7 Debinding profiles for Part C

Run	t_1 (hr)	r_1 (°C/min)	t_2 (hr)	r_2 (°C/min)	t_3 (hr)	Results
1	0	10	0	10	0	Crack, swelling
2	1	6	0	6	0	Crack, swelling
3	0.5	4	0	6	1	Crack

4.2 Compression molded parts

The cylinder-shape samples with a diameter of 15mm but different thickness of 4mm (Part A-1), 8mm (Part A-2), and 12mm (Part A-3) were molded via compression molding (see Fig. 3.1). The feedstock pellet also has cylinder shape, typically with a diameter of 3.5mm and a thickness of 4mm. Therefore the pellets were ground into smaller pieces to improve the mold filling behavior.

One of the drawbacks of compression molding is that it is difficult to make a thick sample due to the occurrence of defects such as voids and segregation, which results from the hydraulic force does not apply on the feedstock homogeneously but on the bottom and top surfaces of the mold. As the water content of the feedstock is approximately 36% in volume, water plays a critical role in molding and debinding. On one hand, water is a carrier for the agar containing mixture that provides flowability and moldability. The presence of water requires venting otherwise it is easily to create defects such as blisters and voids. The water content leads to considerable fluctuations in changes in weight and dimensions. Thus the absolute results of the weight and dimensional changes are not a major concern in this section and will be discussed qualitatively. Furthermore, the

debinding factors were discussed quantitatively in last section, therefore this section mainly focus on the apparent performance of debinding, i.e. visible defects, such as swelling and cracking.

The debinding process parameters and results of compression molded parts are summarized in Appendix C. For the component made of the agar-gel binder system, the debinding process consists of water removal and polymer removal. As can be seen from Appendix C, three initial heating rates as 2, 6 and 10°C/min are used. If the water removal stage is considered as an integral, i.e. air-drying time is discussed combining with initial heating stage, it shows that holding time at room temperature increasing from 0 to 1 hour makes it possible for initial heating rate up to 10°C/min for Part A-1, and 6°C/min initial heating for Part A-2. But as to Part A-3, all the debinding cycles that use an initial heating rate of 6°C/min fail due to cracking or swelling. The initial heating rate is an important factor to successful debinding. The air-drying time for a thin part plays a more important role in water evaporation than for the thick part. This might be attributed to the difference in ratio of surface area to volume. If the water within the compact is removed completely, the secondary heating rate can be triple as the initial heating rate. For example, initial heating as 2 °C/min might follows secondary heating rate as 6°C/min. In addition, the compression molded parts show fluctuated shrinkage in thickness and diameter directions, which might be due to the inconsistent hydraulic force. Therefore the holding time at 110 and 275°C shows less effect in debinding on shrinkage than the effects of molding on the shrinkage.

4.3 Sintered part result

Although debinding is the main concern in the present project, sintering was also explored after the parts are debound. Due to the limited time to use the sintering furnace, only a few selected parts were sintered.

The sintered results of compression molded parts are summarized in Table 4.8. It is well known that the porosity affect the final density, which affects the mechanical strength consequently. Because all the sintering and molding experiments are using the same process parameters, it is reasonable to conclude that the final density is affected by the debinding.

Take Part A-1 for example, the density of Run #17*1 is 7.164 g/cm^3, which is larger than Run #25*1 as 7.089g/cm^3. The difference in debinding is that the holding time at 110°C decreases from 1 hour (Run #17) to 0 (Run #25). This indicates that an increase of holding time at 110°C can improve the development of fine microstructure, consequently increase the final density. In addition, the density of Run #29*1 is 7.239g/cm^3. The difference between Run #29 and Run #25 is that the secondary heating rate. In Run #29*1, the secondary heating rate is 2°C/min while it is 6°C/min in Run #25*1. This shows that slower secondary heating rate improves polymer removal, as a result, increased the final density as well. These sintered density comparisons of Part A-1 approves the previous debinding result discussion.

Similarly, an increase holding time at 110°C from 0 to 1 hour is able to obtain the denser part, as Run #13*2 vs. Run#17*2 (6.925: 6.944 g/cm^3) and Run#25*3 vs. Run #17*3 (6.906: 7.101 g/cm^3). But it should be pointed out that the following table also

shows some comparisons of density do not agree with the previous debinding discussion. This might due to the compression molding stage that already had some voids or segregation, especially for the thick part. Any defects created in previous steps cannot be corrected in the following step in metal injection molding. Therefore the thin Part A-1 shows good accordance to the debinding analysis while the thicker part A-2 and A-3 sometimes show the opposite results.

Table 4.8 Sintered density results and debinding parameters

Run #	H (mm)	T1 (hr)	R1 (°C/min)	T2 (hr)	R2 (°C/min)	T3 (hr)	Final density (g/cm^3)	H%	D%	wt%	Total debinding time (hr)
17*1	4	0	2	1	6	0	7.164	99.999	99.889	6.846	2.21
25*1	4	0	2	0	6	0	7.089	99.833	100.067	7.088	1.21
29*1	4	0	2	0	2	0	7.239	100.329	99.889	6.777	2.13
13*2	8	0	6	0	2	2	6.925	100.079	99.867	7.029	1.63
17*2	8	0	2	1	6	0	6.944	100.840	99.666	7.545	2.21
29*2	8	0	2	0	2	0	6.789	100.328	99.556	7.945	2.13
17*3	12	0	2	1	6	0	7.101	99.866	99.577	7.560	2.21
25*3	12	0	2	0	6	0	6.906	99.678	99.733	7.434	1.21
29*3	12	0	2	0	2	0	6.859	99.390	99.534	7.556	2.13

Chapter 5

CONCLUSIONS

A metal injection molding feedstock with stainless steel and an agar-gel binder system was used to make metal parts with designated shapes by injection molding and compression molding. The parts were debound via various thermal treatments and some samples were further sintered. Based on experimental results and analysis, the main conclusions are given below.

Based on the experiments and fitted statistical models, increased holding times at room temperature, 110°C and 275°C facilitates binder removal. The effects of the first two holding periods in debinding have larger effects than the last holding period, which is in accord with the initial water and polymer content of the feedstock. An increase of holding time at 110°C increases both thickness and diameter shrinkages significantly while increased holding time at 275°C reduces shrinkage in both directions. The initial and secondary heating rates retard binder removal, enhance the thickness shrinkage and reduce the diameter shrinkage. Among the five process parameters, the initial heating rate is most significant factor.

Pre-debinding air-drying time has less influence on binder removal especially for the thicker part; consequently, the thicker part is able to maintain the dimensions better when exposed to the ambient environment.

Initial heating rate is critical in debinding. Especially for thick part sections, acceleration of initial heating rate retards binder removal and decreases thickness and

diameter shrinkages; furthermore, too fast an initial heating rate directly causes visible defects.

Thinner part sections are more sensitive to the effect of holding time at 110°C. Extending the holding time at 110°C is beneficial to obtain better binder extraction and dimensional control.

The secondary debinding stage heating rate has larger effect on thicker part sections in debinding. When accelerating the secondary heating rate, the thinner part shows slight change on debinding result, in contrast, the thicker part shows greater declining gradient on debinding.

For an increase in the holding time at 275°C, the thinner part shows more stable or only slight changes in binder removal and dimensions. In addition, the thicker part has larger effect on diameter than thickness shrinkage.

REFERENCES

Adames, Juan and Leonov, Arkady, "Modeling of water dedinding of metal injection molded parts", SPE ANTEC Tech. Papers, 1575-1579, (2006)

Aggarwal, G.; Park, S. J.; Smid, I., "Development of niobium powder injection molding: Part I. Feedstock and injection molding", International Journal of Refractory Metals & Hard Materials, 24, 253-262 (2006)

Ballard, Clifford; Zedalis, Michael; "Advances in Powder Injection Molding", SPE ANTEC Tech. Papers, 0767, (1998)

Barriere, T.; Gelin, J. C.; Liu, B., "Improving mould design and injection parameters in metal injection moulding by accurate 3D finite element simulation", Materials Processing Technology, 125-126, pp 518-524 (2002)

Barriere, Th.; Liu, B.; Gelin, J. C., "Determination of the optimal process parameters in metal injection molding from experiments and numerical modeling", Materials Processing Technology, 143-144, pp 636-644 (2003)

Chartier, T.; Ferrato, M.; and Baumard, J. F., "Supercritical Debinding of Injection Molded Ceramics", the American Ceramic Society, vol. 78, No. 7, 1787-92 (1995)

Falelli, Anthony; Behi, Mohammad; Ballard, Jr.; Clifford Palmer; Burlew, Joan V, "Gel strength enhancing additives for agaroid-based injection molding compositions", U.S. Patent 5, 746, 957, (1998)

German, R. M., "The production of stainless steels by injection molding water atomized prealloy powders", Injection Molding Technology, Vol. 1, No. 3, 171-180 (1997)

German, R.M.; Bose, A.: Injection Molding of Metals and Ceramics, Metal Powder Industries Federation, Princeton, N.J. (1997)

Haney, Alicyn M., "Development of crosslinkable binder system for metal injection molding using urethane technology", SPE ANTEC Tech. Papers, 1073-1077 (2000)

Haney, A. M. & McConaughy S. D., "Using crosslinked polyethylene to stabilize metal injection molding feedstock", SPE ANTEC Tech. Papers, 3288-3291 (2001)

Hartwig, T. et al. "Powders for Metal Injection Molding", the European Ceramic Society, 18, 1211-1216 (1998)

Hens, K. F.; Kupp, Donald M.; Alexander, Ricky A.; Schofalvi, Karl-Heinz, "Method and binder for use in powder molding", U.S. Patent 5, 332, 537, (1994)

Huang, B., et al., "The rheological and sintering behavior of W-Ni-Fe nano-structured crystalline powder", Materials Processing Technology, 137, 177-182 (2003a)

Huang, B., et al., "The rheology of metal injection molding", Materials Processing Technology, 137, 132-137 (2003b)

Hwang, K.-S., "Fundamentals of Debinding Processes in Powder Injection Molding", Reviews in Particulate Materials, Vol. 4, 71-104, (1996)

Ilinca, F. et al., "3D Simulation of Metal Injection Molding with Free-surface Boundary Conditions: Jetting and Nonuniform Flow", Advances in Powder Metallurgy & Particulate Materials, 4, 73-86, (2000a)

Ilinca, F. et al., "Metal Injection Molding: Simulation of Three-Dimensional Flow with Free Surface Boundary and Experimental Comparison", SPE ANTEC Tech. Papers, 0174, (2000b)

Ilinca, F. et al., "Metal Injection Molding: 3D Modeling of Nonisothermal Filling", Polymer Engineering and Science, Vol. 42, No. 4, 760-770, (2002a)

Ilinca, F. et al., "Three-Dimensional Filling and Post-Filling Simulation of Metal Injection Molding", Journal of Injection Molding Technology, Vol. 6, No. 4, 229-38 (2002b)

Koseski, Ryan P., et al., "Microstructural evolution of injection molded gas- and water-atomized 316L stainless steel powder during sintering", Materials Science and Engineering A 390, 171-177 (2005)

Kwon, Y.- S. et al. "Simulation of the sintering densification and shrinkage behaviour of powder-injection-molded 17-4 PH stainless steel", Metallurgical and materials transaction A, Vol. 35A, 257-263 (2004)

LaSalle, J.C.; Zedalis, M., "Net-shape processing using and aqueous-based MIM binder", JOM, 51 (7), 38-39 (1999).

Li, S., et al., "A new type of binder for metal injection molding", Materials Processing Technology, 137, 70-73 (2003)

Li, Y.; Jiang, F.; Zhao, L.; and Huang, B., "Critical thickness in binder removal process for injection molded compacts", Materials Science and Engineering, A 362, 292-299 (2003)

Lin, H.-K. and Hwang, K.-S., "In Situ Dimensional Changes of Powder Injection –Molded Compacts during Solvent Debinding", Acta Materialia, Vol. 46, No.12, 4303-4309 (1998)

Loh, N. H. and German, R. M., "Statistical analysis of shrinkage variation for powder injection molding", Materials Processing Technology, 59, 278-284 (1996)

Loh, N. H.; Tor, S. B.; Khor, K. A., "Production of metal matrix composite part by powder injection molding", Materials Processing Technology, 108, 398-407 (2001)

MPR, "Combining the best that PIM has to offer to put the bit on a new approach", Technical trend, 22-27, (Nov. 2006)

Omar, M. A., et al., "Rapid debinding of 316L stainless steel injection moulded component", Materials Processing Technology, 140, 397-400 (2003)

Pichot, G., "Powder Injection Molding—Modeling of the debinding stage", McMaster University, (2003)

Rei, M. et al., "Low-pressure injection molding processing of a 316-L stainless steel feedstock", Materials Letters, 52, 360-365 (2002)

Robles, M., "Water debinding in Powder Injection Molding", McMaster University Master thesis (2002)

Shi, Z.; Guo, Z. X.; and Song, J. H., "A diffusion-controlled kinetic model for binder burnout in a powder compact", Acta Materialia, 50, 1937-1950 (2002)

Shimizu, T. et al., "Fabrication of micro-parts by high aspect ratio structuring and metal injection molding using the supercritical debinding method", Microsystem Technologies, 5, 90-92 (1998)

Shimizu, T. et al., "Production of large size parts by MIM process", Materials Processing Technology, 119, 199-202 (2001)

Stevenson, J. F., et al., "Metal Injection Molding: Mold Filling and Packing Dynamics", Advances in Powder Metallurgy & Particulate Materials, 4, 77-91, 2001

Stevenson, J. F.; and Ilinca, F.; and Holmes, B., "Thermally Induced Flow Instability in Metal Injection Molding", Advances in Powder Metallurgy & Particulate Materials, 8, 110-124, (2003)

Stevenson, J. F.; and Ilinca, F., "Thermal Flow Instability in Metal Injection Molding: Experiment and Simulation", Intern. Polymer Processing XXI, 198-210 (2006) 2

Tsai, D.-S. and Chen, W.- W., "Solvent Debinding Kinetics of Alumina Green Bodies by Powder Injection Molding", Ceramics International, 21, 257-264 (1995)

Wick, R.; Ruhland, B.; RTP Co., "Injection more "mettle" into P/M designs", 20 Mar. 2003.http://www.machinedesign.com/ASP/strArticleID/55540/strSite/MDSite/viewSelect edArticle.asp (7 Jun. 2007)

Wu, Y. et al. "Sintering densification and microstructural evolution of injection molding grade 17-4 PH stainless steel powder", Metallurgical and materials transaction A, Vol. 33A, 2185-2194 (2002a)

Wu, Y. et al. "Effect of residual carbon content on sintering shrinkage, microstructure and mechanical propertied of injection molded 17-4 PH stainless steel", Materials Science, 37, 3573-3583 (2002b)

Ying, S. et al., "Two-dimensional simulation of mass transport in polymer removal from a powder injection molding compact by thermal debinding", J. Mater. Res., Vol. 16, No. 8, 2436-2451 (2001)

Ying, S. et al., "Simulation of thermal debinding: effects of mass transport on equivalent stress", Computational Materials Science, 30 496-503 (2004)

Zedalis, M. S. et al., "Stainless steel aqueous molding compositions". U.S. Patent 6, 268, 412, (2001)

APPENDIX A

Calculation of the linear regression fits

Table 4.2 Debinding variables and results of Part B-1

	t_1	r_1	t_2	r_2	t_3	wt %	H%	D%
Run #	(hr)	(°C/min)	(hr)	(°C/min)	(hr)	(%)	(%)	(%)
1	+	-	+	-	+	9.11	0.92	1.4
2	-	-	+	+	+	9.1	0.99	1.26
3	+	+	+	+	-	8.92	0.98	1.46
4	-	+	+	-	-	8.85	2.14	0.942
5	+	-	-	+	-	9.11	1.09	0.71
6	-	-	-	-	-	8.96	0.33	1.17
7avg	+	+	-	-	+	8.97	0.52	1.165
8	-	+	-	+	+	8.7	1.08	0.37

For the ¼ 2^5 design of Part B-1, fit by least squares regression:

$$\beta_i = \frac{\sum (x_i * y_i)}{\sum x_i^2}$$

(1) Effects on binder removal (wt%)

$\beta_0 = 1/8* (y_1 + y_2 + y_3 + y_4 + y_{5+} y_6 + y_7 + y_8)$

$= 1/8* (9.11+9.1+8.92+8.85+9.11+8.96+8.97+8.7)$

80

$$= 8.965$$

$$\beta_1 = 1/8 * (y_1 - y_2 + y3 - y_4 + y_5 - y_6 + y_7 - y_8)$$

$$= 1/8 * (9.11-9.1+8.92-8.85+9.11-8.96+8.97-8.7)$$

$$= 0.0625$$

$$\beta_2 = 1/8 * (-y_1 - y_2 + y3 + y_4 - y_5 - y_6 + y_7 + y_8)$$

$$= 1/8 * (-9.11-9.1+8.92+8.85-9.11-8.96+8.97+8.7)$$

$$= -0.105$$

$$\beta_3 = 1/8 * (y_1 + y_2 + y3 + y_4 - y_5 - y_6 - y_7 - y_8)$$

$$= 1/8 * (9.11+9.1+8.92+8.85-9.11-8.96-8.97-8.7)$$

$$= 0.03$$

$$\beta_4 = 1/8 * (-y_1 + y_2 + y3 - y_4 + y_5 - y_6 - y_7 + y_8)$$

$$= 1/8 * (-9.11+9.1+8.92-8.85+9.11-8.96-8.97+8.7)$$

$$= -0.0075$$

$$\beta_5 = 1/8 * (y_1 + y_2 - y3 - y_4 - y_5 - y_6 + y_7 + y_8)$$

$$= 1/8 * (9.11+9.1-8.92-8.85-9.11-8.96+8.97+8.7)$$

$$= 0.005$$

(2) Effects on thickness shrinkage (H%)

$$\beta_0 = 1/8 * (y_1 + y_2 + y_3 + y_4 + y_5 + y_6 + y_7 + y_8)$$

$$= 1/8 * (0.92+0.99+0.98+2.14+1.09+0.33+0.52+1.08)$$

$$= 1.0063$$

$$\beta_1 = 1/8 * (y_1 - y_2 + y_3 - y_4 + y_5 - y_6 + y_7 - y_8)$$

$$= 1/8* (0.92-0.99+0.98-2.14+1.09-0.33+0.52-1.08)$$

$$= -0.1288$$

$$\beta_2 = 1/8* (-y_1 - y_2 + y_3 + y_4 - y_5 - y_6 + y_7 + y_8)$$

$$= 1/8* (-0.92-0.99+0.98+2.14-1.09-0.33+0.52+1.08)$$

$$= 0.1737$$

$$\beta_3 = 1/8* (y_1 + y_2 + y_3 + y_4 - y_5 - y_6 - y_7 - y_8)$$

$$= 1/8* (0.92+0.99+0.98+2.14-1.09-0.33-0.52-1.08)$$

$$= 0.2513$$

$$\beta_4 = 1/8* (-y_1 + y_2 + y_3 - y_4 + y_5 - y_6 - y_7 + y_8)$$

$$= 1/8* (-0.92+0.99+0.98-2.14+1.09-0.33-0.52+1.08)$$

$$= 0.0287$$

$$\beta_5 = 1/8* (y_1 + y_2 - y_3 - y_4 - y_5 - y_6 + y_7 + y_8)$$

$$= 1/8* (0.92+0.99-0.98-2.14-1.09-0.33+0.52+1.08)$$

$$= -0.1287$$

(3) Effects on diameter shrinkage (D%)

$$\beta_0 = 1/8* (y_1 + y_2 + y_3 + y_4 + y_5 + y_6 + y_7 + y_8)$$

$$= 1/8* (1.4+1.26+1.46+0.942+0.71+1.17+1.165+0.37)$$

$$= 1.0596$$

$$\beta_1 = 1/8* (y_1 - y_2 + y_3 - y_4 + y_5 - y_6 + y_7 - y_8)$$

$$= 1/8* (1.4-1.26+1.46-0.942+0.71-1.17+1.165-0.37)$$

$$= 0.1241$$

$\beta_2 = 1/8* (-y_1 - y_2 + y_3 + y_4 - y_5 - y_6 + y_7 + y_8)$

$= 1/8* (-1.4-1.26+1.46+0.942-0.71-1.17+1.165+0.37)$

$= -0.0754$

$\beta_3 = 1/8* (y_1 + y_2 + y_3 + y_4 - y_5 - y_6 - y_7 - y_8)$

$= 1/8* (1.4+1.26+1.46+0.942-0.71-1.17-1.165-0.37)$

$= 0.2059$

$\beta_4 = 1/8* (-y_1 + y_2 + y_3 - y_4 + y_5 - y_6 - y_7 + y_8)$

$= 1/8* (-1.4+1.26+1.46-0.942+0.71-1.17-1.165+0.37)$

$= -0.1096$

$\beta_5 = 1/8* (y_1 + y_2 - y_3 - y_4 - y_5 - y_6 + y_7 + y_8)$

$= 1/8* (1.4+1.26-1.46-0.942-0.71-1.17+1.165+0.37)$

$= -0.0109$

APPENDIX B

Saturation water vapor pressure at different temperatures

$P_s = 610.78 * \exp (t/(t+238.3) * 17.2694)$ (Pa),

where t is the temperature in °C

Temperature (°C)	Saturation water vapor pressure (Pa)
22	2628.870669
30	4212.101938
40	7309.016703
50	12207.14503
60	19698.55094
70	30815.75198
80	46870.56983
90	69491.63213
100	100659.2086
110	142736.2044

APPENDIX C

Debinding process parameters and results for compression molded parts

Run #	t1	r1	t2	r2	t3	Good-1 Bad-0	Thickness (mm) green parts			Thickness (mm) brown parts			Diameter (mm) green			Diameter (mm) brown			weight (g)		weight loss	Dia-meter	Thick-ness
unit	hr	°C/min	hr	°C/min	hr		center	middle	edge	center	middle	edge	D1	D2	D3	D1	D2	D3	green	brown	wt%	D%	H%
1*1	0	10	1	10	0	0	4.18	4.15	4.12	4.67	4.57	4.19	15	15.03	15	15	15.01	15.03	3.8125	3.5537	6.7882	100.02	107.85
1*2	0	10	1	10	0	0	8.16	8.1	7.93	9.97	9.32	8.1	15.01	15.02	15.01	14.95	15.03	14.99	7.1959	6.6756	7.2305	99.84	113.13
1*3	0	10	1	10	0	0	12.28	12.07	11.99	14.89	12.52	12.27	14.99	14.99	15	14.89	14.99	14.91	10.6289	9.8238	7.5746	99.58	109.11
2*1	1	10	1	10	0	0	4.12	4.07	4.06	4.42	4.21	4.09	15	14.99	15	14.93	14.96	14.96	3.6051	3.346	7.1870	99.69	103.82
2*2	1	10	1	10	0	1	8.14	8.13	8.09	8.19	8.16	8.09	14.99	14.98	14.99	14.94	14.95	14.97	7.1888	6.6567	7.4018	99.78	100.33
2*3	1	10	1	10	0	1	12.32	12.12	12.07	12.58	12.3	12.11	14.99	14.98	14.99	14.95	14.97	14.95	10.6146	9.8497	7.2061	99.80	101.31
3*1	0	10	1	10	2	0	4.1	4	3.98	4.62	4.32	4.03	14.99	15.01	15	14.96	14.98	14.98	3.685	3.436	6.7571	99.82	107.31
3*2	0	10	1	10	2	0	8.2	8.12	7.94	8.59	8.49	8.14	15.01	15.02	15	14.97	14.95	14.98	7.1923	6.6741	7.2049	99.71	103.94
3*3	0	10	1	10	2	0	12.35	12.28	12.14	12.45	12.32	12.32	14.98	14.99	15	n.a.	n.a.	n.a.	10.766	9.9618	7.4698	n.a.	100.87
4*1	1	10	1	10	2	1	4.15	4.09	4.02	4.26	4.13	4.08	14.97	14.98	14.99	14.95	14.96	14.95	3.7011	3.4472	6.8601	99.82	101.71
4*2	1	10	1	10	2	1	8.15	8.21	8.13	8.35	8.25	8.16	14.98	15	14.99	14.96	14.95	14.92	7.2501	6.7216	7.2896	99.69	101.10
4*3	1	10	1	10	2	0	12.17	12.06	11.9	12.3	12.05	12.03	14.99	14.96	14.99	14.86	14.94	14.93	10.4447	9.6506	7.6029	99.53	100.69
29*1	0	2	0	2	0	1	4.12	4.12	4.07	4.12	4.11	4.12	15.01	15.02	15.03	15.01	15.01	14.99	3.7289	3.4762	6.7768	99.89	100.33
29*2	0	2	0	2	0	1	8.13	8.1	8.07	8.2	8.12	8.06	15.02	15.01	15.03	14.97	14.94	14.95	7.061	6.5	7.9451	99.56	100.33
29*3	0	2	0	2	0	1	12.14	12.11	11.94	12.09	12.05	11.83	15.04	15.03	15.02	14.96	14.95	14.97	10.4482	9.6587	7.5563	99.53	99.39
30*1	1	2	0	2	0	1	4.16	4.1	4.07	4.18	4.17	4.1	14.98	14.99	15.02	14.98	15	14.97	3.7617	3.5062	6.7921	99.91	100.98
30*2	1	2	0	2	0	1	8.18	8.16	7.97	8.15	8.13	7.95	14.99	15.02	15.01	14.96	14.96	14.96	7.1638	6.6482	7.1973	99.69	99.67
30*3	1	2	0	2	0	1	12.25	12.22	12.12	12.18	12.04	12.02	15.02	15	15.02	14.93	14.95	14.97	10.4605	9.6574	7.6775	99.58	99.04
31*1	0	2	0	2	2	1	4.12	4.11	4.06	4.09	4.09	4.06	15	15.02	15.02	15	14.99	14.99	3.7021	3.4394	7.0960	99.87	99.60
31*2	0	2	0	2	2	1	8.2	8.11	8.11	8.21	8.12	8.1	15	15.01	15.01	14.98	14.99	14.99	7.1594	6.647	7.1570	99.87	100.04
31*3	0	2	0	2	2	0	12.14	12.03	11.95	12.12	11.98	11.97	14.98	15.02	15.03	15	15	14.99	10.5774	9.7772	7.5652	99.91	99.86
32*1	1	2	0	2	2	1	4.12	4.06	3.96	4.1	4.06	3.98	15	15.03	15.02	14.97	14.98	15	3.6967	3.439	6.9711	99.78	100.01
32*2	1	2	0	2	2	1	8.25	8.12	8	8.25	8.15	8	15	14.98	14.99	15	14.97	14.95	7.168	6.6416	7.3438	99.89	100.12

Run #	t1	r1	t2	r2	t3	Good-1 Bad-0	Thickness (mm) green			Thickness (mm) brown			Diameter (mm) green			Diameter (mm)brown			weight (g)		weight loss	Dia-meter	Thick-ness
unit	hr	°C/min	hr	°C/min	hr		center	middle	edge	center	middle	edge	D1	D2	D3	D1	D2	D3	green	brown	wt%	D%	H%
32*3	1	2	0	2	2	1	12.24	12.04	11.89	12.23	11.96	11.88	14.98	15.01	15.01	14.98	14.96	14.96	10.5773	9.7924	7.4206	99.78	99.72
33*1	0	6	1	6	0	1	4.11	4.08	4.07	4.14	4.08	4.08	15.01	15.02	15.01	14.99	14.98	14.99	3.706	3.4562	6.7404	99.82	100.33
33*2	0	6	1	6	0	1	8.18	8.05	7.97	8.15	8.08	7.98	15.01	14.98	15	14.94	14.97	14.98	7.209	6.6947	7.1341	99.78	100.04
33*3	0	6	1	6	0	0	12.22	12.17	12.05	12.24	12.19	12.11	14.96	14.96	14.93	14.91	14.96	16.1	10.5391	9.7556	12.22	12.17	12.05
34*1	1	6	1	6	0	1	4.12	4.1	4.04	4.12	4.09	4.02	15	15.01	15	14.98	14.97	14.98	3.7192	3.4711	6.6708	99.82	99.75
34*2	1	6	1	6	0	1	8.29	8.25	8.13	8.32	8.17	8.12	14.99	15.01	15.01	14.94	14.96	14.97	7.3113	6.7456	7.7373	99.69	99.76
34*3	1	6	1	6	0	0	12.25	12.18	12.13	12.22	12.22	12.13	14.99	14.98	14.99	14.97	14.97	14.93	10.8505	10.0627	7.2605	99.80	100.03
35*1	0	6	1	6	2	1	4.04	4	3.97	4.19	4.07	4.04	15	15.02	14.99	14.96	14.97	14.99	3.6699	3.4156	6.9293	99.80	102.41
35*2	0	6	1	6	2	0	8.23	8.15	8.05	8.21	8.13	8.1	15	15	14.99	14.98	14.96	14.97	7.2527	6.7478	6.9615	99.82	100.04
35*3	0	6	1	6	2	0	12.24	12.23	12.08	n.a.	n.a.	n.a.	15	14.99	14.98	n.a.	n.a.	n.a.	10.7927	10.0115	7.2382	n.a.	n.a.
36*1	1	6	1	6	2	1	4.16	4.11	4.09	4.22	4.12	4.09	15.01	15.01	15.02	14.96	14.98	14.98	3.7579	3.5076	6.6606	99.73	100.56
36*2	1	6	1	6	2	1	8.18	8.15	8.09	8.18	8.17	8.12	14.98	14.99	15	14.92	14.95	14.93	7.0145	6.5288	6.9242	99.62	100.21
36*3	1	6	1	6	2	0	12.22	12.19	12.1	12.21	12.18	12.11	15	14.98	14.97	14.9	14.94	14.93	10.6345	9.8427	7.4456	99.60	99.97
17*1	0	2	1	6	0	1	4.05	4.04	3.99	4.07	4.03	3.98	14.99	14.99	14.98	14.96	14.98	14.97	3.6648	3.4139	6.8462	99.89	100.00
17*2	0	2	1	6	0	1	8.13	8.04	7.85	8.17	8.07	7.98	14.98	14.93	14.96	14.89	14.91	14.92	6.9055	6.3845	7.5447	99.67	100.84
17*3	0	2	1	6	0	1	12.38	12.31	12.13	12.31	12.33	12.13	14.93	14.97	14.98	14.89	14.91	14.89	10.5838	9.7837	7.5597	99.58	99.87
18*1	1	2	1	6	0	1	4.09	4.03	3.97	4.08	4.06	n.a.	14.99	15.02	15.01	14.99	14.99	15	3.6949	3.4405	6.8852	99.91	100.25
18*2	1	2	1	6	0	1	8.16	8.1	8.01	8.15	8.08	7.98	15.01	15	14.98	14.96	14.95	14.97	7.32114	6.7972	7.1565	99.76	99.75
18*3	1	2	1	6	0	1	12.07	12.02	11.97	12.14	12.03	12.03	14.99	15.01	14.96	14.97	14.89	14.9	10.5566	9.7416	7.7203	99.56	100.39
19*1	0	2	1	6	2	1	4.08	4.02	3.85	4.09	4.05	n.a.	15.02	15.01	14.99	14.97	14.99	14.98	3.7216	3.4627	6.9567	99.82	100.50
19*2	0	2	1	6	2	1	8.01	8.01	7.96	8	7.97	7.96	15.09	15.09	15.11	15.05	15.08	15.07	6.9846	6.4666	7.4163	99.80	99.79
19*3	0	2	1	6	2	1	12.19	12.08	12.03	12.14	12.01	12	14.98	14.98	14.97	14.95	14.95	15	10.5672	9.7557	7.6794	99.93	99.59
20*1	1	2	1	6	2	1	4.1	4.08	4.02	4.09	4.07	4.03	14.97	15.01	15	15	15	14.99	3.81	3.5172	7.6850	100.02	99.92
20*2	1	2	1	6	2	1	8.31	8.3	8.14	8.32	8.28	8.17	14.96	14.97	14.96	14.92	14.91	14.92	7.2512	6.7343	7.1285	99.69	100.08
20*3	1	2	1	6	2	1	12.22	12.16	12.1	12.19	12.16	12.11	14.9	14.95	14.99	14.88	14.92	14.91	10.5252	9.7367	7.4915	99.71	99.95
25*1	0	2	0	6	0	1	4.12	4.11	4.04	4.12	4.12	4.01	14.98	14.99	15.01	15	15	15.01	3.8008	3.5314	7.0880	100.07	99.83
25*2	0	2	0	6	0	1	8.11	8.1	8.07	8.13	8.12	8.12	15.01	14.98	15.01	14.98	14.98	14.99	7.1753	6.6591	7.1941	99.89	100.37
25*3	0	2	0	6	0	1	12.52	12.41	12.28	12.45	12.4	12.24	14.97	14.95	14.94	14.92	14.92	14.9	10.6988	9.9035	7.4335	99.73	99.68
26*1	1	2	0	6	0	1	4.03	4	3.95	4.03	4.01	3.99	14.99	14.99	15	14.98	14.97	14.99	3.5625	3.3088	7.1214	99.91	100.42
26*2	1	2	0	6	0	1	8.26	8.18	8.05	8.24	8.14	8.11	14.99	15	14.95	14.94	14.96	14.95	7.0834	6.5772	7.1463	99.80	100.00

Run #	t1	r1	t2	r2	t3	Good-1 Bad-0	Thickness (mm) green			Thickness (mm) brown			Diameter (mm) green			Diameter (mm)brown			weight (g)		weight loss	Dia-meter	Thick-ness
Unit	hr	°C/min	hr	°C/min	hr		center	middle	edge	center	middle	edge	D1	D2	D3	D1	D2	D3	green	brown	wt%	D%	H%
26*3	1	2	0	6	0	1	12.31	12.23	12.1	12.2	12.16	12.12	14.95	14.98	14.92	14.88	14.89	14.88	10.5066	9.7357	7.3373	99.55	99.57
27*1	0	2	0	6	2	1	4.04	4	3.97	4.05	4.04	4	15	14.99	15	14.98	14.99	14.98	3.6538	3.3985	6.9872	99.91	100.67
27*2	0	2	0	6	2	1	8.15	8.12	8.03	8.15	8.12	8.03	14.99	14.99	15.01	14.9	14.95	14.96	7.05221	6.5349	7.3354	99.60	100
27*3	0	2	0	6	2	1	12.39	12.24	12.11	12.35	12.24	12.1	14.96	14.95	14.96	14.96	14.93	14.89	10.5064	9.7091	7.5887	99.80	99.86
28*1	1	2	0	6	2	1	4.11	4.1	4.01	4.13	4.06	3.99	15	15.01	15.02	14.96	14.99	15.01	3.5653	3.3236	6.7792	99.84	99.67
28*2	1	2	0	6	2	1	8.13	8.11	8	8.14	8.11	8.01	14.99	15	15	14.96	14.97	14.98	7.1782	6.6454	7.4225	99.82	100.08
28*3	1	2	0	6	2	1	12.3	12.22	12.02	12.22	12.16	11.98	15.02	14.96	14.96	14.91	14.93	14.91	10.5712	9.7784	7.4996	99.58	99.51
9*1	0	6	0	6	0	1	4.13	4.11	4.03	4.24	4.16	4.11	14.99	15.01	15.03	15.01	15.02	15.02	3.5856	3.3343	7.0087	100.04	101.96
9*2	0	6	0	6	0	1	8.12	8.06	7.95	8.19	8.12	8.06	15	14.99	14.98	14.94	15.02	15.94	7.1692	6.6564	7.1528	102.07	101.00
9*3	0	6	0	6	0	0	12.37	12.31	12.25	12.38	12.37	12.27	14.96	14.95	14.94	14.93	14.92	15	10.5825	9.8055	7.3423	100	100.24
11*1	0	6	0	6	2	1	4.15	4.12	4.09	4.13	4.09	4.03	15.02	15	14.99	14.96	14.99	14.97	3.5351	3.2986	6.6900	99.80	99.11
11*2	0	6	0	6	2	1	8.28	8.24	8.19	8.2	8.16	8.07	14.98	14.98	14.99	14.96	14.96	14.95	7.171	6.6613	7.1078	99.82	98.87
11*3	0	6	0	6	2	0	12.3	12.31	12.26	12.32	12.28	12.21	14.995	14.95	14.95	14.96	14.97	14.97	10.5755	9.8022	7.3122	100.01	99.84
13*1	0	6	0	2	0	1	4.07	4.05	4	4.24	4.09	4.03	14.99	15.01	15	14.96	14.95	14.99	3.5985	3.3524	6.8390	99.78	101.97
13*2	0	6	0	2	0	1	8.15	8.05	8	8.21	8.06	7.95	14.99	15	15	14.97	14.99	14.97	7.221	6.7134	7.0295	99.87	100.08
13*3	0	6	0	2	0	0	12.08	12.02	11.96	12.16	12.09	n.a.	15	15	15.01	n.a.	n.a.	n.a.	10.5752	9.8058	7.2755	n.a.	n.a.
15*1	1	6	0	2	2	1	4.09	4.07	4.06	4.12	4.07	4.04	15.02	15.03	15.04	15.01	14.99	15.01	3.6884	3.4316	6.9624	99.82	100.08
15*2	1	6	0	2	2	1	8.3	8.21	8.06	8.3	8.2	n.a.	15.02	14.99	15.01	14.99	14.97	15	7.2112	6.6969	7.1320	99.87	99.94
15*3	1	6	0	2	2	0	12.39	12.37	14.25	12.48	12.4	12.24	14.98	14.95	14.96	14.96	14.94	14.91	10.5844	9.7911	7.4950	99.82	95.62
21*1*1	0	2	1	2	0	1	4.1	4.06	4.05	4.11	4.07	4.06	14.99	14.99	15	14.99	14.96	14.97	3.6313	3.3868	6.7331	99.87	100.25
21*1*2	0	2	1	2	0	1	8.24	8.17	8.12	8.25	8.16	8.15	14.98	14.96	14.98	14.92	14.96	14.98	7.2141	6.702	7.0986	99.87	100.12
21*1*3	0	2	1	2	0	1	12.17	12.15	12.12	12.12	12.12	n.a.	15.02	14.04	15.03	14.95	14.98	14.99	10.4334	9.6784	7.2364	101.88	99.67
21*2*1	0	2	1	2	0	1	4.12	4.1	4.05	4.12	4.09	4.02	14.99	14.99	15	14.96	14.98	14.98	3.708	3.4602	6.6828	99.87	99.67
21*2*2	0	2	1	2	0	1	8.19	8.21	8.09	8.19	8.2	8.08	14.96	14.97	15	14.93	14.98	14.97	7.2551	6.7298	7.2404	99.89	99.92
21*2*3	0	2	1	2	0	1	12.48	12.35	14.2	12.35	12.37	n.a.	14.95	14.9	15.01	14.92	14.9	14.89	10.5933	9.8072	7.4207	99.67	99.56
23*1*1	0	2	1	2	2	1	4.18	4.14	4.07	4.21	4.12	4.08	14.99	14.96	15	14.99	14.94	15.03	3.6402	3.396	6.7084	100.02	100.16
23*1*2	0	2	1	2	2	1	8.18	8.15	8.02	8.18	8.16	8.02	14.99	15	15	15.01	14.99	14.99	7.2258	6.7094	7.1466	100	100.04
23*1*3	0	2	1	2	2	1	12.25	12.2	12.01	12.25	12.18	12.02	14.95	14.94	14.99	14.96	14.95	14.97	10.6443	9.8742	7.2349	100	99.97
23*2*1	0	2	1	2	2	1	3.91	3.89	3.8	3.9	3.88	3.83	14.97	14.98	14.95	14.97	14.94	14.99	3.3122	3.0681	7.3697	100	100.09
23*2*2	0	2	1	2	2	1	8.27	8.26	8.16	8.29	8.26	8.15	14.96	14.99	15	14.99	14.98	14.99	7.315	6.809	6.9173	100.02	100.04

Run #	t1	r1	t2	r2	t3	Good-1 Bad-0	Thickness (mm) green			Thickness (mm) brown			Diameter (mm) green			Diameter (mm)brown			weight (g)		weight loss	Dia-meter	Thick-ness
Unit	hr	°C/min	hr	°C/min	hr		center	middle	edge	center	middle	edge	D1	D2	D3	D1	D2	D3	green	brown	wt%	D%	H%
23*2*3	0	2	1	2	2	1	12.22	12.1	12.03	12.12	12.09	12.08	14.93	14.92	14.98	14.94	14.94	14.92	10.3181	9.5594	7.3531	99.93	99.84
5*1*1	0	6	1	2	0	1	4.15	4.13	4.11	4.36	4.22	4.12	14.99	14.99	15	14.99	14.97	14.97	3.6159	3.3644	6.9554	99.89	102.49
5*1*2	0	6	1	2	0	1	8.37	8.27	8.07	8.27	8.2	8.03	14.99	15	14.98	14.93	14.94	14.95	7.0495	6.5075	7.6885	99.67	99.15
5*1*3	0	6	1	2	0	0	12.16	12.04	11.93	12.16	12.01	11.9	14.95	14.98	14.94	14.95	14.96	14.97	10.3284	9.4946	8.0729	100.02	99.83
5*2*1	0	6	1	2	0	1	3.99	3.97	3.88	4.26	3.99	3.91	15	15	14.99	14.98	14.99	14.96	3.5251	3.2736	7.1345	99.87	102.68
5*2*2	0	6	1	2	0	1	8.34	8.22	8.1	8.33	8.25	8.11	14.94	14.96	14.99	14.97	14.88	14.92	7.1362	6.5922	7.6231	99.73	100.12
5*2*3	0	6	1	2	0	0	12.35	12.2	12.09	12.42	12.34	n.a.	14.99	14.93	14.95	n.a.	n.a.	n.a.	10.4378	9.6161	7.8723	n.a.	100.86
7*1*1	0	6	1	2	2	0	4.19	4.17	4.15	5.01	4.37	4.09	14.99	14.96	14.99	14.97	14.95	14.96	3.5174	3.2354	8.0173	99.87	107.64
7*1*2	0	6	1	2	2	1	8.12	8.09	7.93	8.24	8.16	7.95	14.95	14.96	14.97	14.95	14.99	14.92	6.9177	6.3777	7.8061	99.96	100.87
7*1*3	0	6	1	2	2	0	12.09	12.04	11.85	12.23	12.03	11.86	14.92	14.86	14.91	14.86	14.95	14.9	9.853	9.0369	8.2828	100.04	100.39
7*2*1	0	6	1	2	2	1	4.14	4.12	4.08	4.25	4.13	4.09	14.93	14.93	14.94	14.96	14.97	14.93	3.5274	3.2759	7.1299	100.13	101.05
7*2*2	0	6	1	2	2	1	8.3	8.26	8.13	8.39	8.33	8.16	14.95	14.96	14.95	14.94	14.92	14.93	6.9332	6.4046	7.6242	99.84	100.77
7*2*3	0	6	1	2	2	0	12.17	12.13	12.08	14.21	12.22	12.04	14.97	14.94	14.96	14.96	14.95	14.89	10.3717	9.5897	7.5397	99.84	105.72

Debinding process parameters and results for Part B-1

Run #	t1	r1	t2	r2	t3	Thickness (mm) green			Thickness (mm) brown			Diamter (mm)		weight (g)		weight loss	Dia- meter	Thick- ness
Unit	hr	°C/min	hr	°C/min	hr	center	middle	edge	center	middle	edge	Green	Brown	Green	Brown	wt%	D%	H%
1	1.5	0.75	1	1.5	1.6	6.17	6.17	6.03	6.09	6.08	6.03	34.94	34.45	41.8506	38.0363	9.11	0.92	1.4
2	0.5	0.75	1	3	1.6	6.06	6.11	6.04	5.97	6.03	6.03	35.02	34.58	41.9873	38.1684	9.1	0.99	1.26
3	1.5	1.5	1	3	0.8	6.11	6.18	6.03	6.04	6.08	6.02	34.94	34.43	42.0104	38.2616	8.92	0.98	1.46
4	0.5	1.5	1	1.5	0.8	6.07	6.07	6.05	5.9	5.89	6.01	35.02	34.69	42.8181	39.0283	8.85	2.14	0.94
5	1.5	0.75	0.5	3	0.8	6.13	6.15	6	6.05	6.04	5.99	35.03	34.78	41.9637	38.1416	9.11	1.09	0.71
6	0.5	0.75	0.5	1.5	0.8	6.05	6.03	6.03	6.02	6.01	6.02	34.92	34.51	41.4679	37.7522	8.96	0.33	1.17
7	1.5	1.5	0.5	1.5	1.6	6.16	6.14	6.02	6.12	6.11	6.02	34.81	34.41	42.6522	38.8089	9.01	0.38	1.15
7*	1.5	1.5	0.5	1.5	1.6	6.11	6.08	6.02	6.04	6.04	6.01	34.84	34.43	41.7641	38.0332	8.93	0.66	1.18
8	0.5	1.5	0.5	3	1.6	6.17	6.15	6.08	6.07	6.06	6.07	34.77	34.64	42.3878	38.6988	8.7	1.08	0.37

Debinding process parameters and results for Part B-2

Run #	t1	r1	t2	r2	t3	Diameter (mm) Green		Diameter (mm) Brown		Thickness (mm) Green			Thickness (mm) Brown			weight (g)	
unit	hr	°C/min	hr	°C/min	hr	D1	D2	D1	D2	h1	h2	h3	h1	h2	h3	Green	Brown
1	4	0.5	1	1	2	30.24	34.75	30.11	34.59	11.96	11.91	11.71	11.9	11.76	11.56	69.8922	63.771
1*	4	0.5	1	1	2	30.31	34.83	30.09	34.56	11.92	11.85	11.74	11.86	11.74	11.64	69.8192	63.782
2	4	0.5	1	1	0	30.21	34.65	30.05	34.39	12.01	11.86	11.75	11.9	11.72	11.56	69.3294	63.3989
3	2	0.5	1	1	2	30.32	34.88	30.09	34.5	11.97	11.99	11.98	11.81	11.68	11.58	69.5601	63.3626
3*	2	0.5	1	1	2	30.4	35.12	30.09	34.67	12.03	11.93	11.87	11.85	11.77	11.71	70.2224	63.9711
4	2	0.5	1	1	0	30.32	34.93	30.17	34.66	12.04	11.96	11.8	11.9	11.73	11.61	70.0826	63.9302
5	4	0.5	0	1	2	30.44	35.03	30.07	34.55	12.01	11.93	11.85	11.8	11.64	11.61	69.797	63.5373
6	4	0.5	0	1	0	30.39	35.06	30.07	34.67	12.03	12.09	11.92	11.89	11.81	11.62	70.5912	64.3722
7	2	0.5	0	1	2	30.39	34.96	30.11	34.56	11.92	11.9	11.86	11.74	11.61	11.58	70.2319	63.9643
8	2	0.5	0	1	0	30.47	34.99	30.13	34.55	11.94	11.88	11.78	11.73	11.59	11.51	70.0794	63.8718
9	2	0.5	1	2	2	30.41	34.95	30.13	34.54	11.94	11.9	11.82	11.72	11.68	11.69	70.3019	64.1732
10	2	1	1	1	2	30.23	34.78	29.99	34.53	11.98	11.92	11.81	11.9	11.8	11.7	69.8075	63.9001
11	2	1	1	2	2	30.19	34.76	30.02	34.54	11.96	11.83	11.71	11.85	11.73	11.61	69.0215	63.2162

Debinding process parameters and results for Part B-3

Run #	t1	r1	t2	r2	t3	Diameter (mm) Green			Diameter (mm) Brown			Thickness (mm) Green			Thickness (mm) Brown			weight (g)	
unit	hr	°C/ min	hr	°C/ min	hr	D1	D2	D3	D1	D2	D3	h1	h2	h3	h1	h2	h3	Green	Brown
1	4	0.5	1	1	2	25.86	30.59	35.21	25.7	30.45	34.98	17.99	18	17.99	17.89	17.89	17.96	91.413	83.9376
1*	4	0.5	1	1	2	25.8	30.47	35.06	25.52	30.18	34.76	17.9	17.93	17.91	17.77	17.76	17.77	89.601	81.8296
2	4	0.5	1	1	0	25.85	30.59	35.22	25.66	30.39	35.03	18	18.17	18.12	17.92	18.09	17.93	90.901	83.3057
3	2	0.5	1	1	2	25.84	30.55	35.08	25.51	30.29	34.71	17.91	17.94	17.9	17.74	17.63	17.72	89.67	81.9053
3*	2	0.5	1	1	2	25.61	30.23	35.04	25.36	29.99	34.62	18.3	18.42	18.26	18.02	18.1	17.87	89.336	81.5229
4	2	0.5	1	1	0	25.77	30.48	35.01	25.62	30.42	34.97	17.96	17.97	17.96	17.88	17.8	17.81	91.053	83.5335
5	4	0.5	0	1	2	25.82	30.49	35.07	25.53	30.12	34.66	17.91	17.89	17.91	17.71	17.67	17.7	89.663	81.868
6	4	0.5	0	1	0	25.88	30.55	35.14	25.66	30.31	34.86	18.1	17.96	18.09	17.82	17.78	17.82	91.317	83.7951
7	2	0.5	0	1	2	25.75	30.42	35.04	25.47	30.12	34.68	17.94	17.95	17.92	17.68	17.69	17.65	88.894	80.955
8	2	0.5	0	1	0	25.78	30.49	35.04	25.55	30.26	34.76	17.91	17.84	17.92	17.72	17.57	17.71	89.651	81.8025
9	2	0.5	1	2	2	25.86	30.61	35.22	25.65	30.41	34.96	17.96	17.98	17.97	17.83	17.85	17.84	91.799	84.3221
10	2	1	1	1	2	25.79	30.5	35.04	25.53	30.32	34.9	17.99	17.96	17.97		n.a.		91.322	83.8128
11	2	1	1	2	2	25.7	30.41	35.05	25.49	30.21	34.78	17.93	18.01	17.93		n.a.		89.658	82.0056